buildings

MDPI

Article

The Simplified Method of Head Stiffness Considering Semi-Rigid Behaviors of Deep Foundations in OWT Systems

Wei Li [1], Xiaojuan Li [2,*], Tengfei Wang [2], Qian Yin [3] and Mingxing Zhu [2]

[1] School of Electrical Engineering, Guangxi University, Nanning 530004, China; 2012401002@st.gxu.edu.cn
[2] School of Civil Engineering and Architecture, Jiangsu University of Science and Technology, Zhenjiang 212003, China; 221110901121@stu.just.edu.cn (T.W.); mxingzhu@just.edu.cn (M.Z.)
[3] School of Civil Engineering, Southeast University, Nanjing 211189, China; 230198808@seu.edu.cn
* Correspondence: xiaojuan_li@just.edu.cn

Abstract: Simplified methods of static free head stiffness of the semi-rigid foundation under lateral loads were limited to flexible or rigid behavior by the critical length of piles. This would lead to errors when predicting the static or dynamic performance of their upper structures in OWT Systems. This paper presents a comprehensive analysis of the head static stiffness of the semi-rigid pile without considering the critical length. Firstly, case studies using the energy-based variational method encompassing nearly twenty thousand cases were conducted. These cases involved different types of foundations, including steel pipe piles and concrete caissons, in three types of soil: homogeneous soil, linearly inhomogeneous soil, and heterogeneous soil. Through the analysis of these cases, a series of polynomial equations of three kinds of head static stiffness, containing the relative stiffness of the pile and soil, the slenderness ratio, and Poisson's ratio, were developed to capture the semi-rigid behavior of the foundations. Furthermore, the lateral deflection, the rotation for concrete caissons in the bridge projects, and several natural frequencies of three cases about the OWT system considering the SSI effect were carried out. the error of high-order frequency of the OWT system reached 13% after considering the semi-rigid effect of the foundation.

Keywords: deep foundations; lateral loads; offshore geotechnical engineering; semi-rigid behavior; soil-structure interaction (SSI) effect

Citation: Li, W.; Li, X.; Wang, T.; Yin, Q.; Zhu, M. The Simplified Method of Head Stiffness Considering Semi-Rigid Behaviors of Deep Foundations in OWT Systems. *Buildings* **2024**, *14*, 1803. https://doi.org/10.3390/buildings14061803

Academic Editor: Eugeniusz Koda

Received: 19 April 2024
Revised: 25 May 2024
Accepted: 7 June 2024
Published: 14 June 2024

1. Introduction

Monopiles and well foundations (also known as caissons), with large diameters (2 m $\leq D \leq$ 10 m) and smaller slender ratios ($2 \leq L_p/D \leq 10$, L_p is the length of the foundation), are extensively employed in offshore structures or bridges (Figure 1). The circular cross-sections of these foundations are designed as massive hollow bodies to comply with mechanics and reduce costs [1–3]. These foundations carry mechanisms of lateral loads to the surrounding soils caused by wind, waves, and earthquakes, and bring great challenges to predicting the supporting performance. It is important to note that the laterally loaded foundation belongs to a semi-rigid beam, which both covers rigid and flexible behavior (Figure 1). The soil-structure interaction (SSI) effect can lead to changes in the static or dynamic mechanical behavior of the upper structures, and the effect would be much more obvious when involving high-order derivative operations [4–7]. On the other hand, Structural monitoring or real-time analysis of dynamics leads to an urgent need for a more accurate expression of the SSI effect. Therefore, to maintain the stability and serviceability of a structure, it is imperative to accurately predict the foundation's free-head stiffness under lateral loads. This precision is particularly critical for preserving the accuracy of upper structure results during high-order derivative mechanical calculations, especially when accounting for the SSI effect.

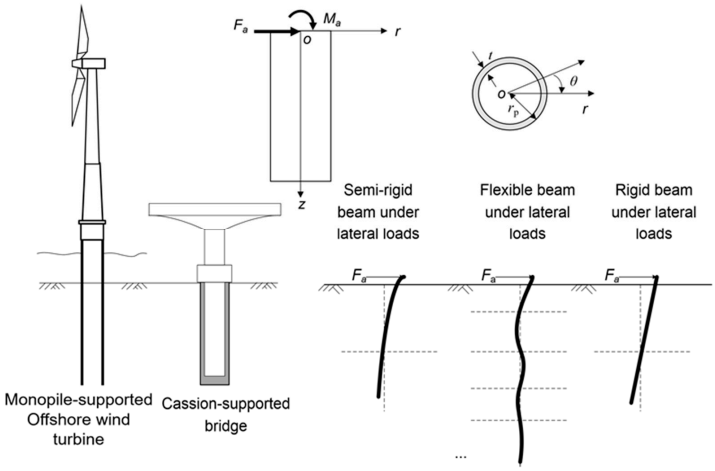

Figure 1. The bending behavior of a semi-rigid beam, a flexible beam, and a rigid beam in offshore or bridge projects (free-end boundary condition).

The free head stiffness of a foundation under lateral loads is commonly characterized by three parameters: K_L (lateral stiffness), K_R (rocking stiffness), and K_{LR} (cross-coupling stiffness). The critical length of piles, typically determined as a function of the relative stiffness between the pile and soil, plays a pivotal role in influencing foundation performance [8–10]. Depending on the specified threshold value for the critical length, various beam theories are employed to model the foundation's bending behavior. Consequently, different equations for K_L, K_R, and K_{LR} are utilized. These stiffness parameters, particularly their initial values, serve two key purposes: firstly, they are instrumental in predicting the foundation's head deflection and rotation under static loading conditions; secondly, they are essential for factoring in the Soil-Structure Interaction (SSI) effect during dynamic analysis, particularly within the framework of a Serviceability Limit State (SLS).

To characterize the head stiffness of laterally loaded piles, researchers have explored several approaches over the decades, including closed-form solutions based on Winkler-based theory, semi-analytical analyses grounded in continuum theory, and experimental testing. Tables 1 and 2 provide a compilation of key findings from these studies. For example, Bergfelt [11] proposed a closed function of K_L based on the long flexible beam in a Winkler foundation. Building upon this work, Thomas [12] provided a solution considering the relative stiffness of the pile and soil. Randolph [13] developed the finite element method to modify the 3-D continuum behavior of the soil and put forward equations for K_L, K_R, and K_{LR} in flexible and rigid beams based on the relative stiffness of the pile and soil (E_{eq}/E_s). Additionally, Poulos and Davis [14], following Barber [15], presented a series of functions for K_L, K_R, and K_{LR}, considering flexible and rigid beams with the threshold value of β. Other researchers, such as Budhu and Davies [16], Pender [17], Gazetas [18], Higgins et al. [19], Shadlou and Bhattacharya [20], Aissa et al. [21]. and Anoyatis et al. [22], have proposed expressions for flexible piles and rigid piles. These studies collectively yield dimensionless expressions for K_L, K_{LR}, and K_R, which are denoted as $K_L/(E_sD)$, $K_{LR}/(E_sD^2)$, and $K_R/(E_sD^3)$, respectively. Notably, these investigations reveal that the dimensionless head stiffness of long, flexible piles is primarily influenced by the parameter E_{eq}/E_s, while for short piles, the slenderness ratio (L_p/D) assumes a significant role. However, the foundations examined in this study primarily exhibit semi-rigid beam characteristics, demonstrating aspects of both rigid and flexible behavior. Specifically, when predicting the static or dynamic performance of upper structures—particularly those involving high-order derivative operations like high-order self-resonant frequencies—traditional methods may yield results with significant, non-negligible errors [23]. Therefore, there is a compelling need to develop a more precise equation for calculating the dimensionless head stiffness—those that consider both the rigid and flexible behavior of the foundation while remaining as practical to calculate as the methods employed in previous studies.

Table 1. Different equations of stiffness formula by different researchers for Semi-infinite beams in various soil profile. m* is the equivalent ratio of shear modulus, $m^* = dGs/dz(1 + 0.75\nu s)$

Source	K_L, K_R and K_{LR} (If Have)	Constant Value				Beam and Soil Material
		K_L	K_{LR}	K_R	Others	
Randolph [13], Ko [24]		$a_1 = 3.147$ $b_1 = 1/7$	$a_2 = -0.5311$ $b_2 = 3/7$	$a_3 = 0.2458$ $b_3 = 5/7$	$E_{eq} = \frac{E_p I_p}{\frac{\pi D^4}{64}}$ $f(\nu_s) = \frac{1+0.75\nu_s}{1+\nu_s}$ E_{s0} is the initial value of soil elastic modulus	The Semi-infinite beam in homogeneous and linear inhomogeneous soils (Triangular-linear strain element)
Pender [17]		$a_1 = 1.285$ $b_1 = 0.188$	$a_2 = -0.3075$ $b_2 = 0.47$	$a_3 = 0.18125$ $b_3 = 0.738$		The Semi-infinite beam in homogeneous soil
		$a_1 = 0.85$ $b_1 = 0.29$	$a_2 = -0.24$ $b_2 = 0.53$	$a_3 = 0.15$ $b_3 = 0.77$		The Semi-infinite beam in linear inhomogeneous homogeneous soil
		$a_1 = 0.735$ $b_1 = 0.33$	$a_2 = -0.27$ $b_2 = 0.55$	$a_3 = 0.1725$ $b_3 = 0.776$		The Semi-infinite beam in parabolic inhomogeneous soil
Gazetas [18] and Eurocode 8 Part 5 [25]	K_L: $a_1 E_{s0} D f(\nu_s) \left(\frac{E_{eq}}{E_{s0}}\right)^{b_1}$ K_{LR}: $a_2 E_{s0} D^2 f(\nu_s) \left(\frac{E_{eq}}{E_{s0}}\right)^{b_2}$ K_R: $a_3 E_{s0} D^3 f(\nu_s) \left(\frac{E_{eq}}{E_{s0}}\right)^{b_3}$	$a_1 = 1.08$ $b_1 = 0.21$	$a_2 = -0.22$ $b_2 = 0.50$	$a_3 = 0.16$ $b_3 = 0.75$	$f(v_s) = 1$ m^* is the equivalent ratio of shear modulus, $m^* = dG_s/dz(1 + 0.75\nu_s)$	The Semi-infinite beam in homogeneous soil
		$a_1 = 0.60$ $b_1 = 0.35$	$a_2 = -0.17$ $b_2 = 0.60$	$a_3 = 0.14$ $b_3 = 0.80$		The Semi-infinite beam in linear inhomogeneous soil
		$a_1 = 0.79$ $b_1 = 0.28$	$a_2 = -0.24$ $b_2 = 0.53$	$a_3 = 0.15$ $b_3 = 0.77$		The Semi-infinite beam in parabolic inhomogeneous soil
		$a_1 = 0.1967\ m^*$ $b_1 = 18$	$a_2 = -0.3472\ m^*$ $b_2 = 0.43$	$a_3 = 0.2083\ m^*$ $b_3 = 0.72$		-
		a_1=0.1967 m^* $b_1 = 33$	a_2=−0.3472 m^* $b_2 = 0.54$	a_3=0.2083 m^* $b_3 = 0.78$		-
Syngros [26]; Anoyatis [22]		$a_1 = 1.24$ $b_1 = 0.18$	$a_2 = -0.21$ $b_2 = 0.50$	$a_3 = 0.15$ $b_3 = 0.75$		The Semi-infinite beam in parabolic inhomogeneous soil
Shadlou et al. [20]		$a_1 = 1.45$ $b_1 = 0.186$	$a_2 = -0.30$ $b_2 = 0.50$	$a_3 = 0.18$ $b_3 = 0.73$	$f(\nu_s) = \frac{1}{1+\nu_s-0.25}$	The Semi-infinite beam in homogeneous soil
		$a_1 = 0.79$ $b_1 = 0.34$	$a_2 = -0.26$ $b_2 = 0.567$	$a_3 = 0.17$ $b_3 = 0.78$		The Semi-infinite beam in linear inhomogeneous homogeneous soil
		$a_1 = 1.02$ $b_1 = 0.27$	$a_2 = -0.29$ $b_2 = 0.52$	$a_3 = 0.17$ $b_3 = 0.76$		The Semi-infinite beam in parabolic inhomogeneous soil

Table 1. *Cont.*

Source	K_L, K_R and K_{LR} (If Have)	Constant Value				Beam and Soil Material
		K_L	K_{LR}	K_R	Others	
Higgins et al. [19]	$K_L = \frac{100G_s r_p \left(\frac{E_p}{E_s}\right)^{0.18}}{3.4-\left(\frac{E_p}{E_s}\right)^{0.04}} K_{LR} = \frac{1}{0.3}\frac{G_s r_p^2 \left(\frac{E_p}{E_s}\right)^{0.47}}{\left(\frac{E_p}{E_s}\right)^{0.04}-3.4} K_R = \frac{34}{9}\frac{G_s r_p^3 \left(\frac{E_p}{E_s}\right)^{0.72}}{3.4-\left(\frac{E_p}{E_s}\right)^{0.04}}$					The Semi-infinite beam in homogeneous soil
	$K_L = \frac{1.23 m^* r_p^2 \left(\frac{E_p}{m^* r_p}\right)^{0.33}}{0.6765-0.2704\left(\frac{E_p}{m^* r_p}\right)^{0.03}} K_{LR} = \frac{0.52 m^* r_p^3 \left(\frac{E_p}{m^* r_p}\right)^{0.57}}{0.2704\left(\frac{E_p}{m^* r_p}\right)^{0.03}-0.6765} K_R = \frac{0.55 m^* r_p^4 \left(\frac{E_p}{m^* r_p}\right)^{0.78}}{0.6765-0.2704\left(\frac{E_p}{m^* r_p}\right)^{0.03}}$				$f(\nu_s) = G_s(1 + 0.75\nu_s)/E_s$ $m^* = dG_s/dz(1 + 0.75\nu_s)$	The Semi-infinite beam in linear inhomogeneous soil
		a_1 = 3\3.66\4.58 (L_p/r_p = 40, E_p/E_s = 100\300\1000)	a_2 = 2.70\4.48\7.81 (L_p/r_p = 6, E_p/E_s = 100~1000	a_3 = 6.02\13.20\31.31 (L_p/r_p = 6, E_p/E_s = 100~1000)		-

Table 2. Different equations of Stiffness formulae by different researchers for short beams in various soil profile.

Source	K_L, K_R and K_{LR} (If Have)	Constant Value			Others	Beam and Soil Material
		K_L	K_{LR}	K_R		
Randolph [13], Ko [24]	K_L: $a_1 E_{s0} D f(\nu_s) \left(\frac{E_{eq}}{E_{s0}}\right)^{b_1}$ K_{LR}: $a_2 E_{s0} D^2 f(\nu_s) \left(\frac{E_{eq}}{E_{s0}}\right)^{b_2}$ K_R: $a_3 E_{s0} D^3 f(\nu_s) \left(\frac{E_{eq}}{E_{s0}}\right)^{b_3}$	$a_1 = 3.150/(1 - 0.3345(L_p/D)^{0.25}$ $b_1 = 1/3$	$a_2 = -2.045/(1 - 0.3345(L_p/D)^{0.25}$ $b_2 = 9/8$	$a_3 = 3.969/(1 - 0.3345(L_p/D)^{0.25}$ $b_3 = 5/3$	Finite element method	The rigid beam in homogeneous and linear inhomogeneous soils (Triangular-linear strain element)
Carter and Kulhawy [27]; Bouzid et al. [28]		$a_1 = 1.884$ $b_1 = 0.627$	$a_2 = -1.048$ $b_2 = 1.483$	$a_3 = 1.91$ $b_3 = 2.049$		The rigid beam in homogeneous soil
Higgns et al. [19]; Bouzid et al. [28]		$a_1 = 2.426$ $b_1 = 0.71$	$a_2 = -1.44$ $b_2 = 1.67$	$a_3 = 1.789$ $b_3 = 2.459$	The Fourier finite-element method	The rigid beam in homogeneous soil
		$a_1 = 0.929$ $b_1 = 2.041$	$a_2 = -0.633$ $b_2 = 3.061$	$a_3 = 0.672$ $b_3 = 3.491$		The rigid beam in linear inhomogeneous soil
Shadlou and Bhattacharya [20]		$a_1 = 3.2$ $b_1 = 0.62$	$a_2 = -1.7$ $b_2 = 1.56$	$a_3 = 1.65$ $b_3 = 2.5$	3D element analysis	The rigid beam in homogeneous soil
		$a_1 = 2.35$ $b_1 = 1.53$	$a_2 = -1.775$ $b_2 = 2.5$	$a_3 = 1.58$ $b_3 = 3.45$		The rigid beam in linear inhomogeneous soil
		$a_1 = 2.66$ $b_1 = 1.07$	$a_2 = -1.8$ $b_2 = 2.0$	$a_3 = 1.63$ $b_3 = 3.0$		The rigid beam in parabolic inhomogeneous soil
Abed et al. [29]; Bouzid et al. [28]		$a_1 = 1.708$ $b_1 = 1.661$	$a_2 = -1.233$ $b_2 = 2.655$	$a_3 = 0.672$ $b_3 = 3.941$	Fourier Series Aided Finite Element (FSAFE) approach	The rigid beam in linear inhomogeneous soil
		$a_1 = 2.841$ $b_1 = 0.977$	$a_2 = -2.933$ $b_2 = 1.767$	$a_3 = 3.894$ $b_3 = 2.562$		The rigid beam in soil whose stiffness increases with the square root of the depth
Aissa et al. [21]		$a_1 = 2.756$ $b_1 = 0.668$	$a_2 = -1.595$ $b_2 = 1.636$	$a_3 = 1.731$ $b_3 = 2.495$	The semi-analytical finite element analysis	The rigid beam in homogeneous soil
Carter et al. [27]		K_L: $\frac{3.15 G_s^* D^{\frac{2}{3}} L_p^{\frac{1}{3}}}{1-0.28\left(\frac{2L_p}{D}\right)^{\frac{1}{4}}}$	K_{LR} : $-\frac{2 G_s^* D^{\frac{7}{8}} L_p^{\frac{5}{3}}}{1-0.28\left(\frac{2L_p}{D}\right)^{\frac{1}{4}}}$	K_R : $\frac{4 G_s^* D^{\frac{4}{3}} L_p^{\frac{5}{3}}}{1-0.28\left(\frac{2L_p}{D}\right)^{\frac{1}{4}}}$	G^* is the equivalent shear modulus, $G^* = G_s$ (1 + 0.75 ν_s)	The rigid beam in bedrock

The energy-based variational method, characterized by its energy-based theory and virtual work principles, has emerged as a valuable approach for predicting the response of piles subjected to lateral loads. This method offers notable advantages, combining the efficiency of quick computations with the mathematical rigor comparable to that of three-dimensional finite-difference analyses [30–32]. Previously, Shadlou et al. [20] conducted an energy-based study that involved the modification of pile-head spring stiffness (K_L, K_R, and K_{LR}) using the Euler-Bernoulli beam theory in layered soils. As highlighted in previous research (Byron & Houlsby [33,34]; Gupta [35–37], Cao [38]), the Timoshenko beam model has gained recognition for its appropriateness in characterizing the response of laterally loaded piles with substantial diameters. More intricate models, such as shells or solid bodies, have found application in commercial software like ABAQUS, FLAC3D, or PLAXIS. A consensus has emerged within the research community, affirming that the Timoshenko beam strikes a commendable balance between accuracy and simplicity. Gupta [37] and Gupta and Basu [36] introduced the Timoshenko beam theory within the energy-based variational method, discussing pile-head spring stiffness under both dynamic and static lateral loads with no specific calculation equations provided in this work; Taking the method further, Li [39–43] extended its application by considering both vertical and horizontal soil displacement in the analysis of laterally loaded deep foundations.

The objective of this research is to investigate the head static stiffness of the semi-rigid pile without the critical length. To achieve this, a comprehensive study using the energy-based variational method with Timoshenko beam encompassing nearly twenty thousand cases was conducted. By using the efficiency of the variational method, different types of foundations (steel pipe piles and concrete caissons) with diameters and slenderness ratios (L_p/D) ranging from 2 m to 10 m, and three types of soil (homogeneous soil, linearly inhomogeneous soil, and heterogeneous soil) were studied, each characterized by varying elastic moduli and Poisson's ratio. Through the analysis of these cases, the three kinds of static stiffness of the pile head, covering the relative stiffness of the pile and soil, the slenderness ratio as well and Poisson's ratio without consideration of the critical length, were developed to accurately capture the semi-rigid behavior exhibited by these foundations. These new equations can ensure the accuracy of mechanical calculation involving high-order derivative operations of the upper structures.

2. Methodology

2.1. Energy-Based Variational Method

The energy-based variational method has the advantage of computational efficiency and open accessibility. To investigate the head stiffness of a semi-rigid pile, we examine a single circular beam, which may represent either a pile or a caisson. This beam has specific geometric parameters, including a radius (r_p), wall thickness (t), and length (L_p), and it is embedded within a three-dimensional continuous medium. The beam experiences lateral forces (F_a) and/or moments (M_a) at its head (Figure 1). In this analysis, we treat the pile as a vertical Timoshenko beam, characterized by a lateral deflection denoted as $w(z)$, which is associated with the depth parameter z. and the shear rotation of the plane section is $\phi(z)$, the three-dimensional soil displacement distribution can be simplified as below in terms of r-θ-z:

$$\begin{aligned} u_r &= w(z)\phi_r(r)\cos\theta \\ u_\theta &= -w(z)\phi_\theta(r)\sin\theta \\ u_r &= \phi(z)r_p\phi_z(r)\cos\theta \end{aligned} \tag{1}$$

The boundary conditions of ϕ_r, ϕ_θ, and ϕ_z are given as:

$$\phi_r(r) = \begin{cases} 1 & 0 \le r \le r_p \\ 0 & r \to \infty \end{cases}$$
$$\phi_\theta(r) = \begin{cases} 1 & 0 \le r \le r_p \\ 0 & r \to \infty \end{cases}$$
$$\phi_z(r) = \begin{cases} 0 & r_p = 0 \\ \frac{r}{r_p} & 0 < r < r_p \\ 1 & r = r_p \\ 0 & r \to \infty \end{cases} \quad (2)$$

where $\phi_z(r_\mathrm{p})$ is the value of $\phi_z(r)$ when $r = r_\mathrm{p}$. In Equation (2), the functions ϕ_r and ϕ_θ both have a value of 1 when $0 \le r \le r_\mathrm{p}$ and 0 when r approaches infinity. As for ϕ_z, it equals 0 when r is 0 and r/r_p when $0 < r < r_\mathrm{p}$, ϕ_z becomes 0 again as r approaches infinity. These functions are related to the variables r, θ, and the pile radius r_p. In Equation (2), it is further assumed that ϕ_r, ϕ_θ, and ϕ_z are mutually independent in the r-direction. The boundary condition of ϕ_z at $0 \le r \le r_\mathrm{p}$ is from the static Timoshenko beam theory (Timoshenko, 1932; https://ccrma.stanford.edu/~bilbao/master/node163.html, accessed on 16 February 2024.), where the displacements of the beam are $u_r = w(z)\cos\theta$, $u_\theta = -w(z)\sin\theta$, and $u_z = \phi(z)\cos\theta$.

For Timoshenko beam theory, depending on the total energy of the system and the principle of virtual work, the following equation is obtained:

$$\delta\prod = E_\mathrm{p}I_\mathrm{p}\int_0^{L_\mathrm{p}}\left(\frac{\mathrm{d}\phi}{\mathrm{d}z}\right)\delta\left(\frac{\mathrm{d}\phi}{\mathrm{d}z}\right)\mathrm{d}z + \int_0^{L_\mathrm{p}}\kappa G_\mathrm{p}A_\mathrm{p}\left(\frac{\mathrm{d}w}{\mathrm{d}z} - \phi\right)\delta\left(\frac{\mathrm{d}w}{\mathrm{d}z} - \phi\right)\mathrm{d}z + \int_0^{L_\mathrm{p}}\int_0^{2\pi}\int_{r_\mathrm{p}}^{\infty}\sigma_{pq}\delta\varepsilon_{pq}r\mathrm{d}r\mathrm{d}\theta\mathrm{d}z + \int_{L_\mathrm{p}}^{\infty}\int_0^{2\pi}\int_0^{\infty}\sigma_{pq}\delta\varepsilon_{pq}r\mathrm{d}r\mathrm{d}\theta\mathrm{d}z - \delta W \quad (3)$$

where E_p is Young's modulus of the beam; I_p is the second moment of inertia of the cross-section; κ is the shear correction factor; w is the lateral displacement of the beam central line; W is the work by outer force (lateral force F_a or moment M_a). The soil potential energy is in the region of $r > r_\mathrm{p}$ when $L_\mathrm{p} \ge z \ge 0$ and $r > 0$ when $z \ge L_\mathrm{p}$; σ_{pq} is the stress in soil domain; ε_{pq} is the strain in soil domain.

2.2. Soil Conditions

To obtain the initial stiffness, the soil is in an elastic state under very small to small strain conditions, and the stress-strain relationship is elastic. In this section, four main categories are considered from the point of view of the current analysis:

(1) **Homogenous soil conditions** ($E_\mathrm{s} = E_{\mathrm{s}0}(z/D)^\alpha$, $\alpha = 0$): $E_{\mathrm{s}0}$ is the initial value of soil elastic modulus, α is an index of the function. The elastic modulus is considered constant with a depth of the soil, often used in cohesive soils, weathered bedrock, and very dense sand for typical North Sea soils [7,44].

(2) **Lineally inhomogeneous soil conditions** ($E_\mathrm{s} = E_{\mathrm{s}0}(z/D)^\alpha$, $\alpha = 1$): G_s increases linearly with depth from zero value at the ground surface, also called Gibson's soil, often used to describe normally consolidated cohesive soils [7], London clay reported by Skempton and Henkel [45], see also, Ward et al. [46], Burland and Lord [47], Butler [48], and Hobbs [49].

(3) **Heterogeneous soil conditions** ($E_\mathrm{s} = E_{\mathrm{s}0}(z/D)^\alpha$, $0 < \alpha < 1$): G_s increases nonlinearly with depth from zero value at the ground surface; when $\alpha = 0.5$, it is described as a parabolic soil profile, which has been used to describe soil profiles in several Europe offshore wind projects [7,50].

(4) **Complex layered soil conditions**: E_s is obviously not included in the above categories, different layers with obviously different E_s are often observed, and often used in real sites, the multilayered sedimentation in river or coast areas, i.e., interlaced layers with soft clay and sand. There are other soil conditions characterized by heterogeneity,

such as $G = G_1 + G_2 \cos(z/D)$. These conditions often arise in geomaterials formed through periodic deposition, such as varved clays and sedimentary rocks [51].

This paper primarily centers its attention on deep foundation scenarios that pertain to bridges and offshore structures. These scenarios are categorized within groups (1) to (3). In elastic media, the constitutive model is $\sigma_{pq} = \lambda_s(z)\delta_{pq}\varepsilon_{pp} + 2G_s(z)\varepsilon_{pq}$ (p, q = 1, 2, 3), where $\lambda_s(z)$ and $G_s(z)$ are Lame's constants; $\lambda_s = E_s v_s/(1 + v_s)/(1 - 2v_s)$; $G_s = E_s/2/(1 + v_s)$; E_s is the elastic modulus; v_s is Poisson's ratio. Therefore, λ_s in categories (1) to (3) can be given by:

$$\lambda_s = \frac{E_{s0}\nu_s(z/D)^{\alpha}}{(1+\nu_s)(1-2\nu_s)} \tag{4}$$

2.3. Governing Differential Equations of the Beam and Soils

The governing differential equations of the foundation and soils have been derived in the Appendices A and B, the governing differential equations of soils have been derived in the Appendix C. The stiffness of a beam under lateral loading is expressed in matrix form as follows:

$$\begin{bmatrix} K_L & K_{LR} \\ K_{RL} & K_R \end{bmatrix} \begin{bmatrix} w_{z=0} \\ \left(\frac{dw}{dz}\right)_{z=0} \end{bmatrix} = \begin{bmatrix} F \\ M \end{bmatrix} \tag{5}$$

where K_L is the swaying dynamic head stiffness, K_{LR} is the coupled swaying-rocking head stiffness, and K_R is the rocking dynamic head stiffness $K_{LR} = K_{RL}$.

To calculate K_L, K_{LR}, and K_R, three steps are needed:

(1) A response analysis with applied lateral force F_a and restricted pile head rotation θ to derive the lateral stiffness coefficient ($K_L = F_a/w_0$), the boundary conditions at the pile head are F_a = *constant*, $\theta_0 = 0$, w_0 is unknown, and

$$\begin{aligned} &\kappa G_p A_p\left(\tfrac{dw}{dz} - \phi\right) + k_2\phi + 2t\tfrac{dw}{dz} = -F_a \quad (z = 0\ \mathrm{m}) \\ &\theta_0 = \tfrac{dw}{dz} = 0 \end{aligned} \tag{6}$$

where t and k_2 are shown in Appendix A.

(2) A response analysis for calculating to moment M_a that leads to zero rotation θ for a given pile head displacement w_0. This defines the off-diagonal term ($K_{LR} = -M_a/w_0$), the boundary conditions at the pile head are w_0 = *constant*, $\theta_0 = 0$, M_a is unknown, and

$$\begin{aligned} &w_0 = \text{constant} \quad (z = 0\ \mathrm{m}) \\ &\theta_0 = 0 \end{aligned} \tag{7}$$

(3) A response analysis with zero pile head deflection w_0 and an applied bending moment M_a. The rotational stiffness coefficient can be derived from the observed pile head rotation ($K_R = -M_a/\theta$) the boundary conditions at the pile head are M_a = *constant*, $w_0 = 0$, θ_0 is unknown, and

$$\begin{aligned} &w_0 = 0 \quad (z = 0\ \mathrm{m}) \\ &E_p I_p \tfrac{d\phi}{dz} + (-k_1 + k_2)w + 2t_4\tfrac{d\phi}{dz} = M_a \end{aligned} \tag{8}$$

where k_1, k_2 and t_4 are shown in Appendix A.

From Equations (1)–(8), the values of K_L, K_{LR}, and K_R can be obtained, respectively. The derivation details are given in Appendix B.

2.4. Modeling Cases

The values of K_L, K_{LR}, and K_R are influenced by a multitude of factors, including the diameter of the pile (D), the slenderness ratio (L_p/D), the thickness of the pile wall (t), the relative stiffness of the pile and soil, the elastic modulus of the soil (E_s), and Poisson's ratio (v_s). To comprehensively explore the impact of these parameters, a wide range of values has been considered in the analyses conducted for this paper, as summarized in Table 3. For instance, the wall thickness for monopiles typically falls within the range

of $D/80$ to $D/120$, equivalent to $0.005D$ to $0.015D$ [14]. In the case of concrete caissons, the wall thickness is in the range of $0.05D$ to $0.15D$. Additionally, the elastic modulus of the soil (E_{s0}) has been studied within the range of 2 MPa to 300 MPa, Poisson's ratio (v_s) spans from 0.20 to 0.45. In fact, this study has examined over twenty thousand cases to comprehensively investigate the relationships and effects of these parameters on K_L, K_{LR}, and K_R. These cases encompass a wide array of deep foundation scenarios pertinent to bridges and offshore structures, ensuring a thorough exploration of the subject matter.

Table 3. Pile geometries and soil conditions in study cases.

Pile Diameter D (m)	Slenderness Ratio, L_p/D	Diameter-to-Wall Thickness Ratio	Elastic Modulus		v_s
			Pile (E_p) GPa	Soil (E_s)	
2–10	2–10	$t = (0.01 \pm 0.005)D$	210 (Steel pipe pile)	$E_s = E_{s0}(z/D)^{\alpha}$	0.20–0.45
2–10	2–10	$t = (0.1 \pm 0.05)D$	30 (Concrete caissons)	(α = 0, 0.25, 05, 0.75, 1)	

3. Results and Discussion

3.1. Validation of the Analysis Compared against Different Methods

Homogenous soil conditions (α = 0) To investigate the influence of $\ln(E_{eq}/E_s)$ and L_p/D on the head stiffness of laterally loaded foundations in homogeneous soil conditions, we present Figures 2–4 as illustrative examples. These figures depict the effects of $\ln(E_{eq}/E_s)$ and L_p/D on $K_L/(E_sD)$, $K_{LR}/(E_sD^2)$, and $K_{LR}/(E_sD^3)$ for steel monopiles, considering $t = 0.01D$ and $v_s = 0.30$ in 3-D version. The results are compared with closed-form solutions from Randolph [13], Shadlou et al. [20], Higgins et al. [19], and Abed et al. [29] presented in Tables 1 and 2.

As presented in previous studies, Randolph [13] and Carter et al. [27] respectively proposed the critical pile length of slender piles and rigid piles as:

$$\frac{L_p}{D}\begin{cases} \geq \left(\frac{E_{eq}}{E_s(1+0.75v_s)/(1+v_s)}\right)^{2/7} & \text{flexible piles} \\ \leq 0.05\left(\frac{E_{eq}}{E_s(1+0.75v_s)/(1+v_s)}\right)^{1/2} & \text{rigid piles} \end{cases} \tag{9}$$

Then Higgins et al. [19] proposed a method for determining flexible pile and rigid piles with the consideration of:

$$\frac{L_p}{D}\begin{cases} \geq 40 & \text{flexible piles} \\ \leq \left(\frac{1}{412.8}\frac{E_{eq}}{E_s(1+0.75v_s)/(1+v_s)}\right)^{1/3.23} & \text{rigid piles} \end{cases} \quad (\alpha = 0) \tag{10}$$

and

$$\frac{L_p}{D} \leq \left(\frac{1}{650}\frac{E_{eq}}{\frac{dE_s}{dz}D(1+0.5v_s)/(1+v_s)}\right)^{1/3.45} \quad \text{rigid piles} \quad (\alpha = 1) \tag{11}$$

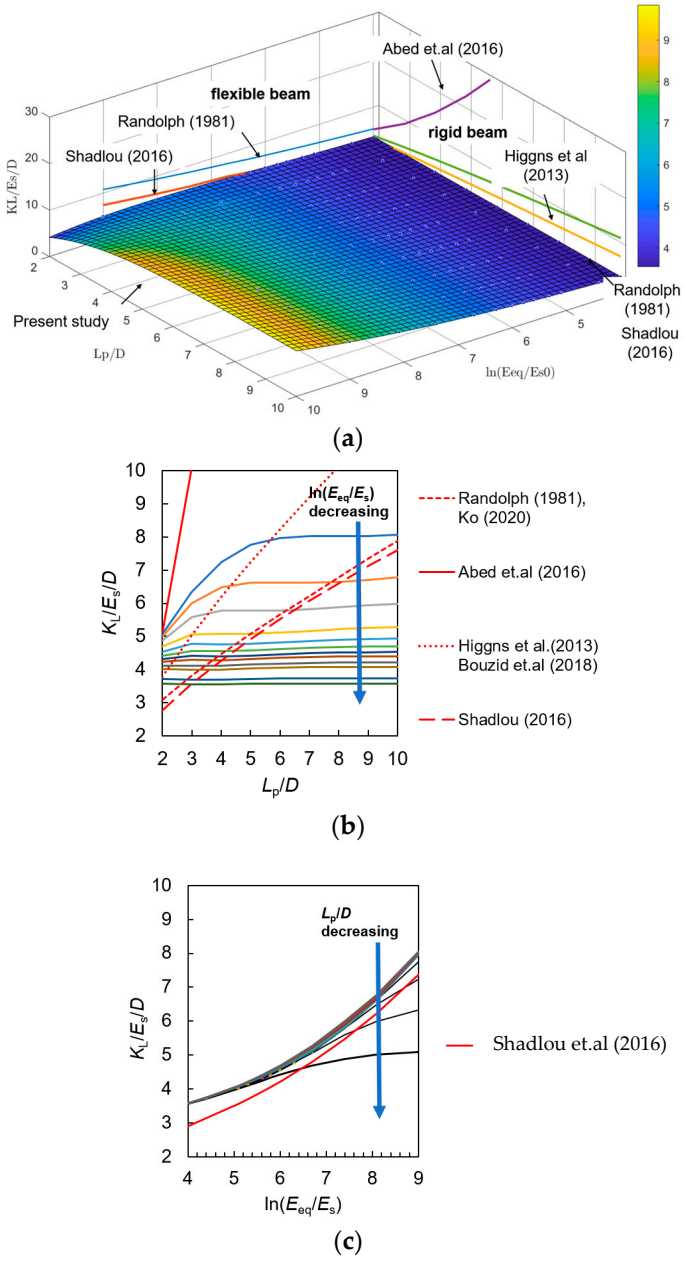

Figure 2. The results of $KL/(E_sD)$ at (**a**) 3-D, (**b**) L_p/D and (**c**) $\ln(E_{eq}/E_s)$ version in homogenous soil conditions compared with different methods ($t = 0.01D$, $v_s = 0.30$).

Figure 3a illustrates a similar relationship between $K_{LR}/(E_sD^2)$ and both (L_p/D) and $\ln(E_{eq}/E_s)$ in the 3-D context. Figure 3b highlights the trend of decreasing values of $K_{LR}/(E_sD^2)$ with increasing L_p/D for short piles ($2 \leq L_p/D \leq 6$, $\ln(E_{eq}/E_s) > 4.5$). These values are consistent with those from Randolph [13] and Shadlou et al. [20] for rigid piles, falling within the range of $K_{LR}/(E_sD^2)$ values obtained in the present study. However, the rate of increase differs: the former exhibits a positive increasing rate concerning (L_p/D), while the results from this study indicate that $K_{LR}/(E_sD^2)$ becomes insensitive to L_p/D when $L_p/D \geq 6$, suggesting a flexible pile behavior. The successful prediction of the threshold zone where $K_{LR}/(E_sD^2)$ becomes insensitive to L_p/D by Higgins et al. [19] further supports this observation. In Figure 3c, the equations provided by Shadlou et al. [20] and Randolph [13] for flexible piles in Table 1 also demonstrate good performance on $K_{LR}/(E_sD^2)$ when $L_p/D \geq 6$.

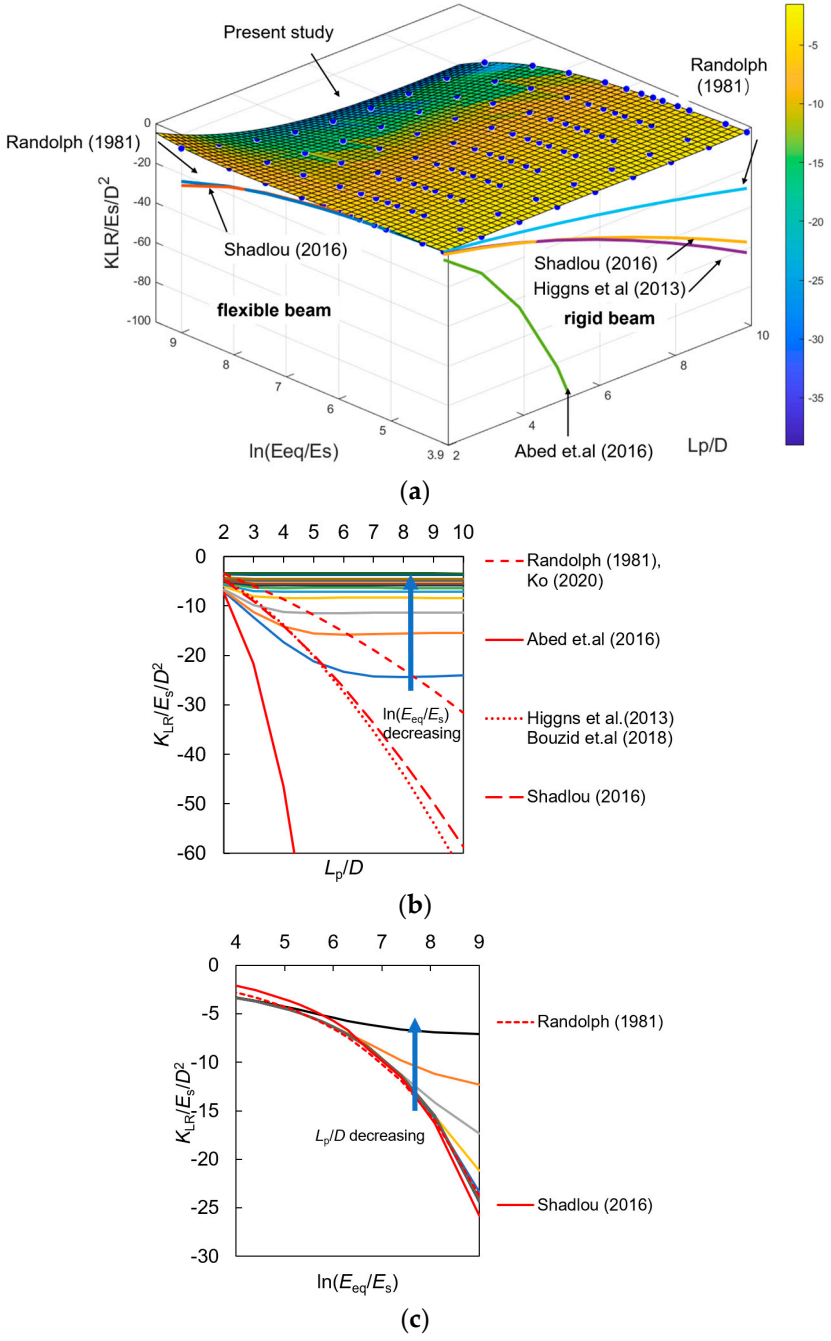

Figure 3. The results of $KLR/(E_sD^2)$ at (**a**) 3-D, (**b**) L_p/D and (**c**) $\ln(E_{eq}/E_s)$ version in homogenous soil conditions compared with different methods ($t = 0.01D$, $v_s = 0.30$).

A similar phenomenon is also evident in Figure 4, where the relationship between $K_R/(E_sD^3)$ and (L_p/D) and $\ln(E_{eq}/E_s)$ in the 3-D context has been analyzed. This phenomenon has also been observed in the case of concrete caissons.

Based on the findings presented in Figures 2–4, it can be concluded that while traditional methods demonstrate good performance for $K_L/(E_sD)$, $K_{LR}/(E_sD^2)$, and $K_R/(E_sD^3)$, it is essential for the functions of $K_L/(E_sD)$, $K_{LR}/(E_sD^2)$, and $K_R/(E_sD^3)$ to incorporate the parameters E_{eq}/E_s and L_p/D. Therefore, the development of more accurate equations that consider both parameters is warranted. These observations highlight the need for more comprehensive and refined equations that account for a broader range of influencing factors, ultimately improving our ability to predict the head stiffness of laterally loaded foundations in various scenarios.

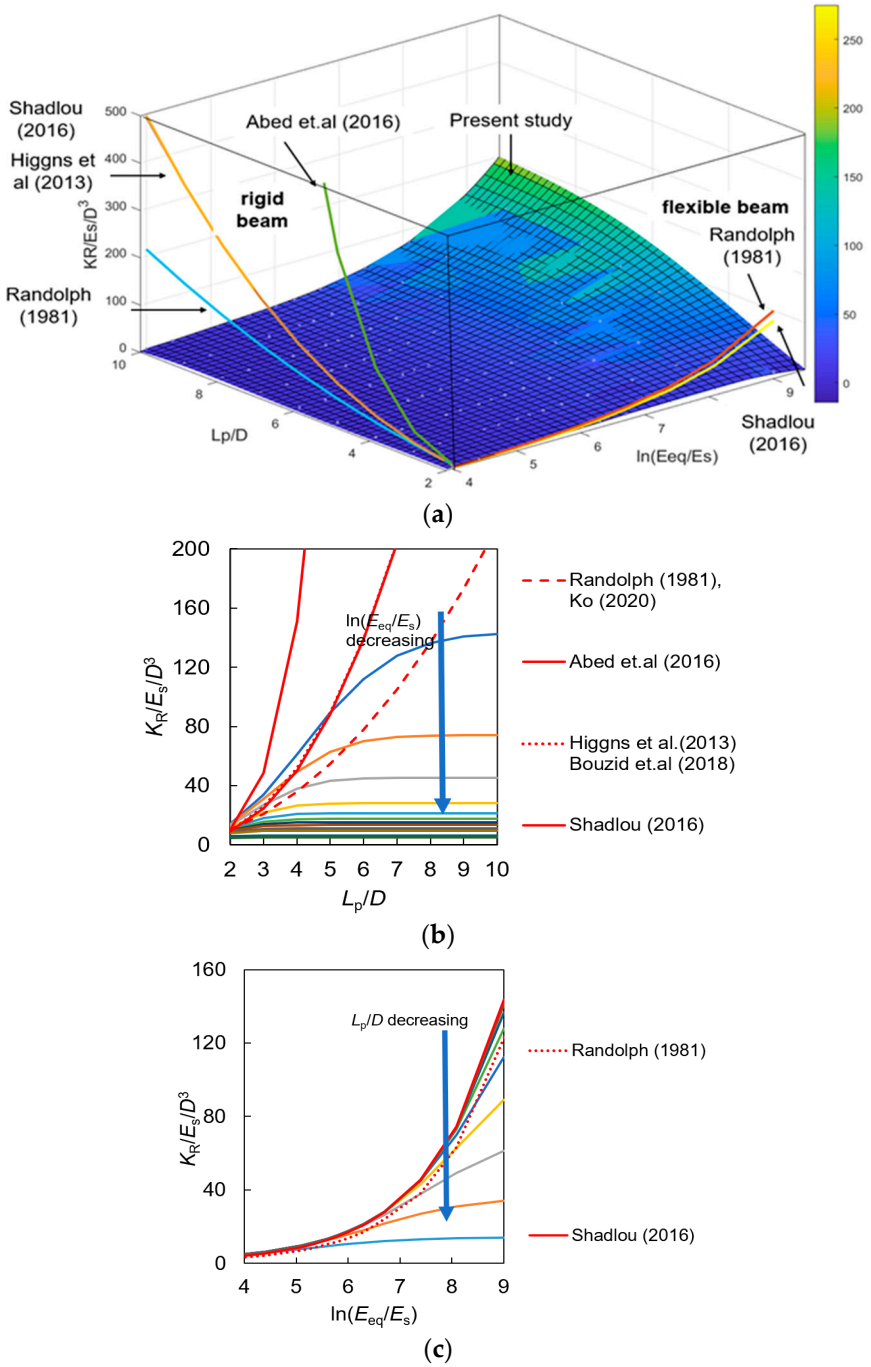

Figure 4. The results of $K_R/(E_sD^3)$ at (**a**) 3-D, (**b**) L_p/D and (**c**) $\ln(E_{eq}/E_s)$ version in homogenous soil conditions compared with different methods ($t = 0.01D$, $v_s = 0.30$).

Linearly inhomogeneous soil conditions (α = 1). To comprehend the impact of $\ln(E_{eq}/E_s)$ and L_p/D on the head stiffness of laterally loaded foundations in linearly inhomogeneous soil conditions, Figures 5–7 provide insights into the effects of these parameters on $K_L/(E_sD)$, $K_{LR}/(E_sD^2)$, and $K_{LR}/(E_sD^3)$ for steel monopiles with $t = 0.01D$ and $v_s = 0.30$. In Figure 5a, it is evident that the results presented in this study are influenced by $\ln(E_{eq}/E_s)$ and L_p/D. Figure 5b demonstrates that $K_L/(E_sD)$ for short piles ($2 \leq L_p/D \leq 4$, $\ln(E_{eq}/E_s) \geq 6$) exhibits an increasing trend with rising L_p/D values, aligning well with the results from Shadlou et al. [20], Higgins et al. [19], Abed et al. [29] for rigid pile conditions in Table 2. Conversely, results from Randolph [13] tend to underpredict $K_L/(E_sD)$ at smaller L_p/D values, while those from Higgins et al. [19], Shadlou et al. [20], and Abed et al. [29]

tend to overpredict it at larger L_p/D values. In Figure 5c, it becomes evident that $K_L/(E_sD)$ becomes less sensitive to L_p/D as $\ln(E_{eq}/E_s)$ decreases and L_p/D increases. This behavior indicates a flexible pile response. The threshold zone where $K_L/(E_sD)$ becomes insensitive to L_p/D is successfully predicted by Higgins et al. [19], and equations from Pender [17] and Shadlou et al. [20] for flexible piles perform better in terms of prediction accuracy compared to the equation from Randolph [13].

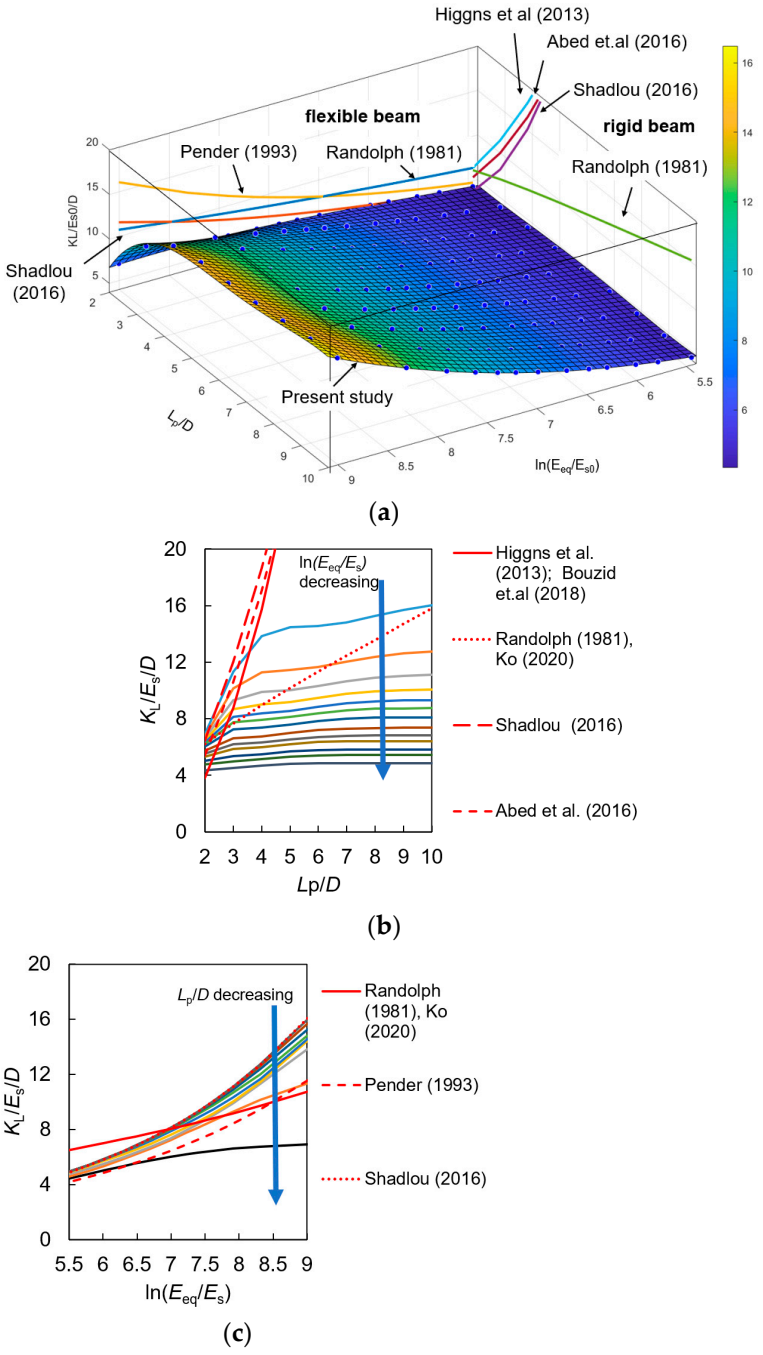

Figure 5. The results of $K_L/(E_sD)$ at (**a**) 3-D, (**b**) L_p/D and (**c**) $\ln(E_{eq}/E_s)$ version in linearly inhomogeneous soil conditions compared with different methods ($t = 0.01D$, $v_s = 0.30$).

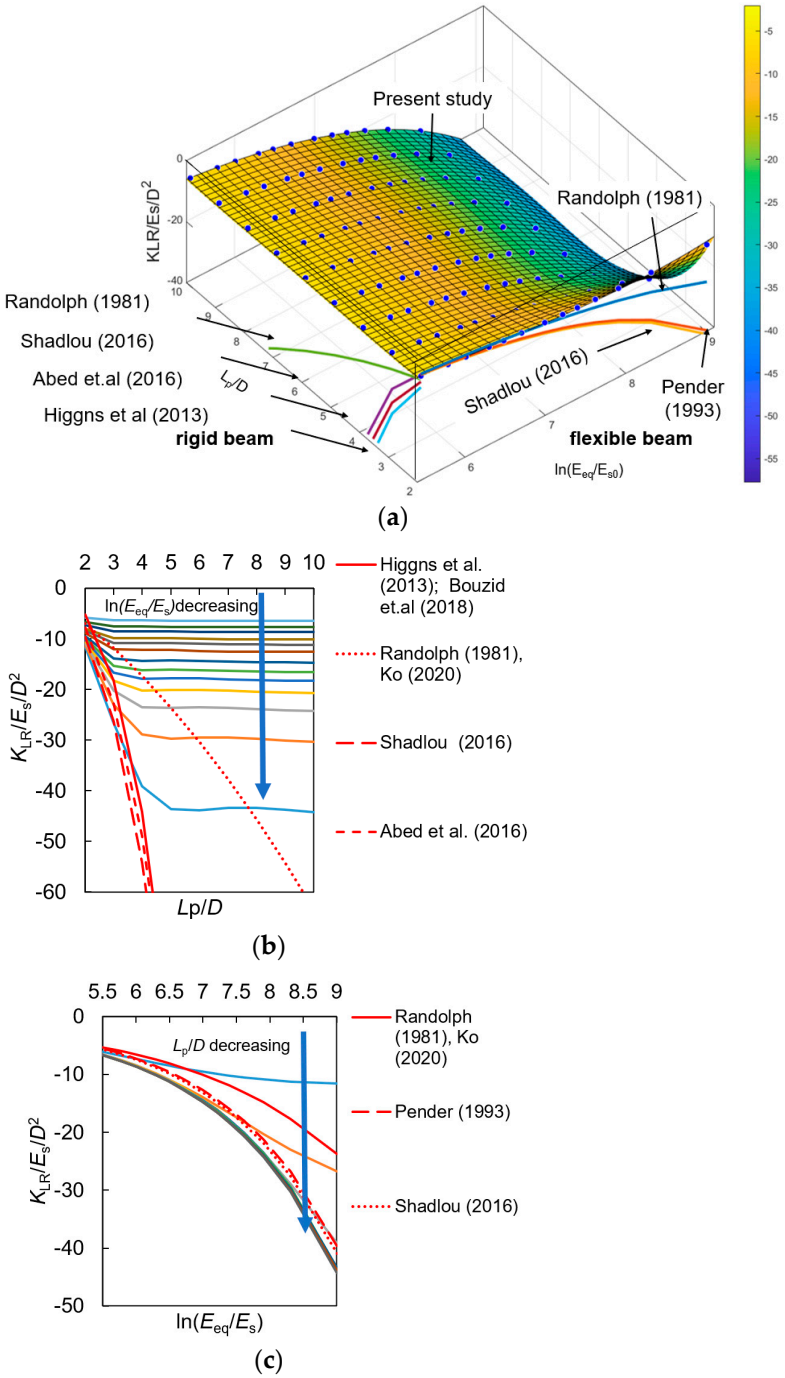

Figure 6. The results of $KLR/(E_sD^2)$ at (**a**) 3-D, (**b**) L_p/D and (**c**) $\ln(E_{eq}/E_s)$ version in linearly inhomogeneous soil conditions compared with different methods ($t = 0.01D$, $v_s = 0.30$).

Figure 6 demonstrates a similar relationship between $K_{LR}/(E_sD^2)$ and both (L_p/D) and $\ln(E_{eq}/E_s)$ in the 3-D context. In Figure 6a, it's evident that the results presented in this study are influenced by $\ln(E_{eq}/E_s)$ and L_p/D. Figure 6b illustrates that for short piles ($2 \leq L_p/D \leq 4$, $\ln(E_{eq}/E_s) > 6$), the values of $K_{LR}/(E_sD^2)$ exhibit a curvilinear decrease as L_p/D increases. The range of L_p/D values ($2 \leq L_p/D \leq 4$) covered by the results from the present study for $K_{LR}/(E_sD^2)$ includes the results from Randolph [13], Higgins et al. [19], Shadlou et al. [20], and Abed et al. [29] for rigid pile conditions. Similar to the previous case, as L_p/D increases beyond 6, $K_{LR}/(E_sD^2)$ becomes insensitive to L_p/D, with the threshold zone falling between the predictions of Randolph [13] and Higgins et al. [19]. In Figure 6c, the results from this paper at $L_p/D = 3$ align more closely with the predictions for flexible

piles by Randolph [13] (as given in Table 1), while the results from the present study for $L_p/D \geq 6$ better match the equations from Shadlou et al. [20] and Pender [17] for flexible piles (as given in Table 1). A similar trend is observed in Figure 6, where $K_R/(E_sD^3)$ versus (L_p/D, ln (E_{eq}/E_s)) in the 3-D version was analyzed, and the same phenomenon has also been observed in concrete well foundations (or caissons).

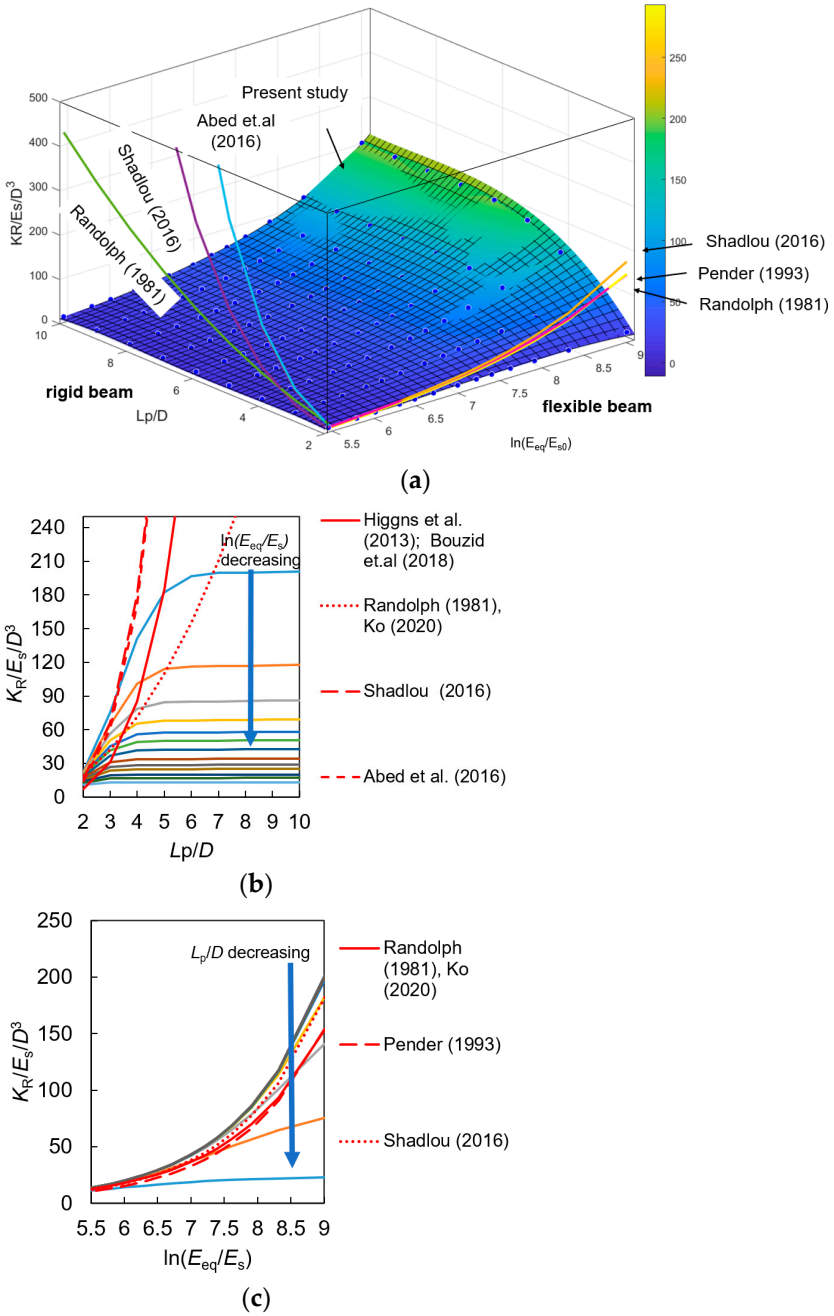

Figure 7. The results of $KR/(E_sD^3)$ at (**a**) 3-D, (**b**) L_p/D and (**c**) ln(E_{eq}/E_s) version in linearly inhomogeneous soil conditions compared with different methods (t = 0.01D, v_s = 0.30).

Based on the insights provided in Figures 5–7, it becomes evident that the relationships governing $K_L/(E_sD)$, $K_{LR}/(E_sD^2)$, and $K_R/(E_sD^3)$ should be expressed as functions of both E_{eq}/E_s and L_p/D when dealing with linearly inhomogeneous soils. This underscores the need for more precise equations that take into account the combined influence of these two parameters. It's worth noting that the threshold zones for long flexible piles and short

rigid piles in linearly inhomogeneous soils differ from those observed in homogeneous soils, indicating the importance of considering soil heterogeneity in foundation analysis.

Heterogeneous soil conditions (α = 0.5). Figures 8–10 provide insights into the impact of ln (E_{eq}/E_s) and L_p/D on $K_L/(E_sD)$, $K_{LR}/(E_sD^2)$, and $K_{LR}/(E_sD^3)$ for steel monopiles with $t = 0.01D$ and $v_s = 0.30$. In Figure 8a, it is evident that the results presented in this study are influenced by ln(E_{eq}/E_s) and L_p/D. Figure 8b shows that the values of $K_L/(E_sD)$ for short piles exhibit an increasing trend with rising L_p/D values, and the results at $L_p/D = 2$ and ln(E_{eq}/E_s) = 9.08 align well with those of Shadlou et al. [20] for rigid pile conditions, as presented in Tables 1 and 2. In Figure 8c, $K_L/(E_sD)$ becomes less sensitive to L_p/D as ln(E_{eq}/E_s) decreases and L_p/D increases, indicating a foundation behavior more akin to a flexible pile. The values from the present study at $L_p/D = 2$ are closer to those from Syngros [26], and the values at $L_p/D > 5$ fall within the range between the equations from Gazetas [18] and the equations from Shadlou et al. [20] used for flexible piles.

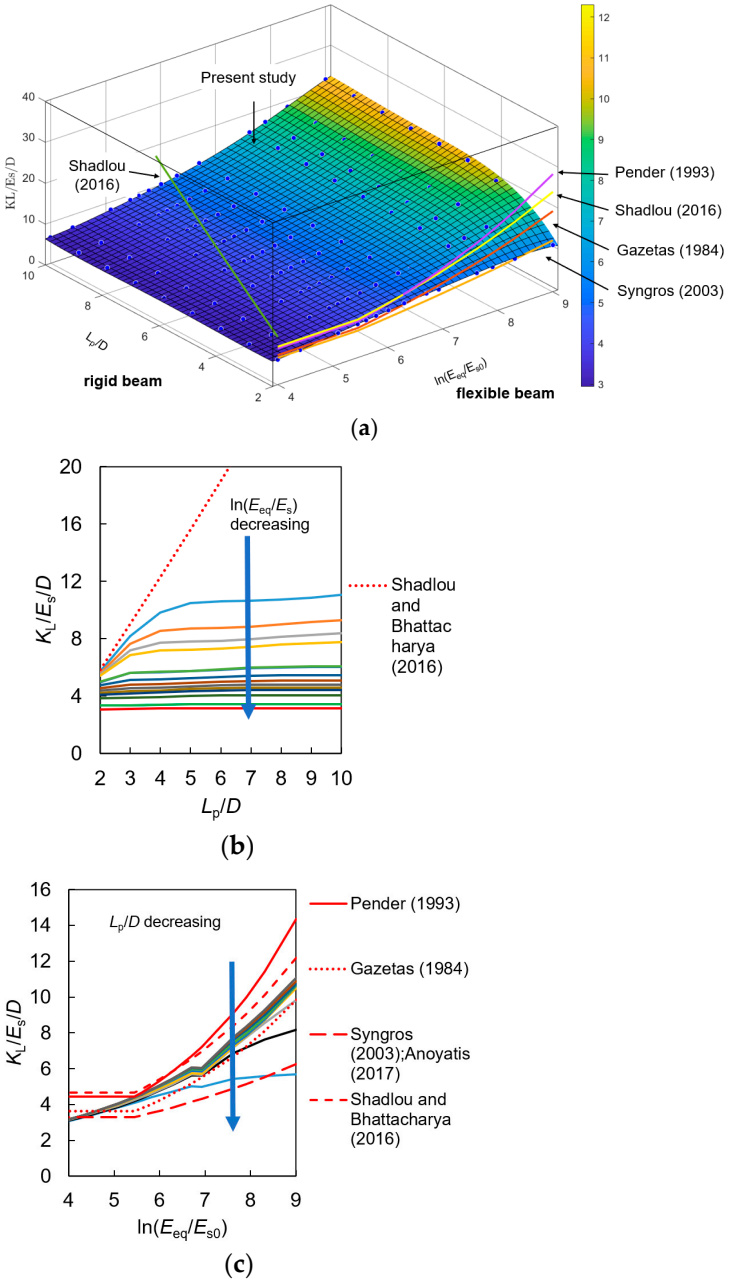

Figure 8. The results of $K_L/(E_sD)$ at (**a**) 3-D, (**b**) L_p/D and (**c**) ln(E_{eq}/E_s) version in homogenous soil conditions compared with different methods ($t = 0.01D$, v_s = 0.25–0.35).

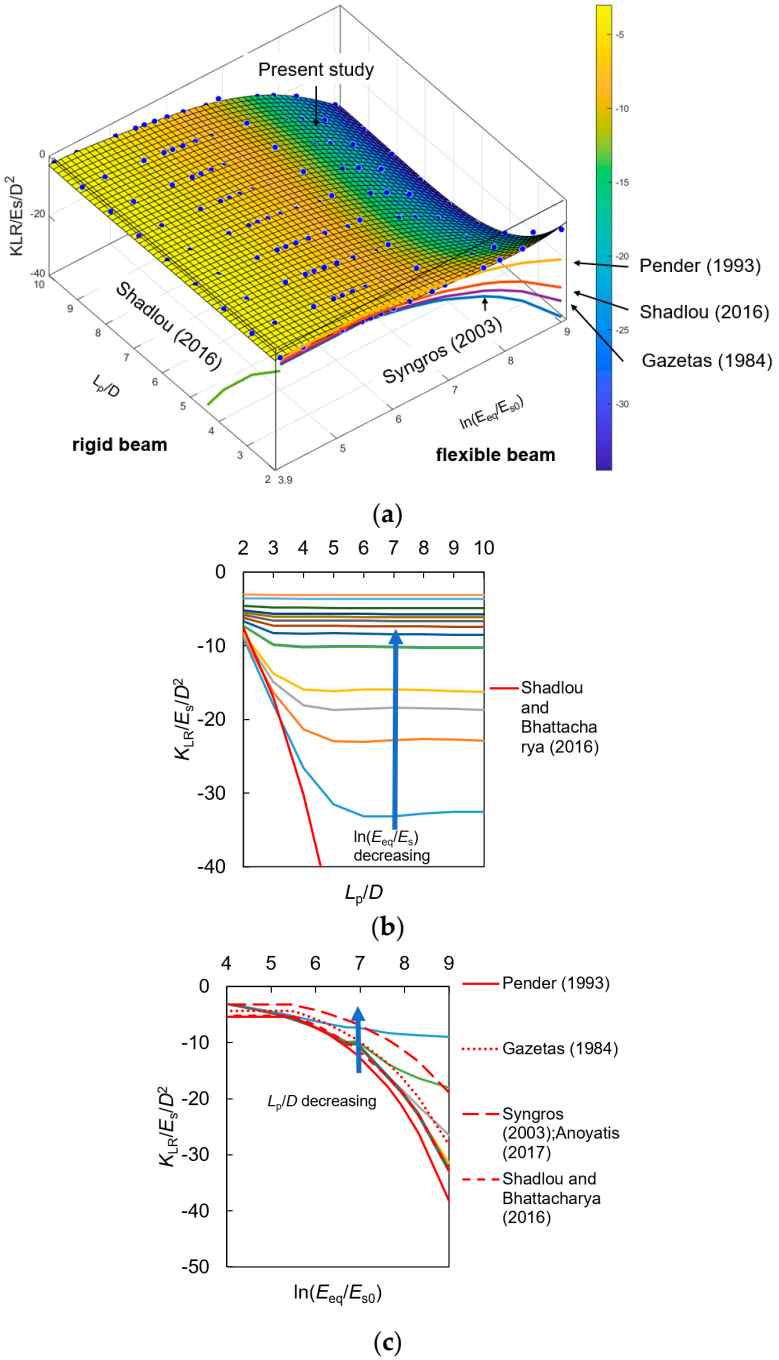

Figure 9. The results of $K_{LR}/(E_sD^2)$ at (**a**) 3-D, (**b**) L_p/D and (**c**) $\ln(E_{eq}/E_s)$ version in heterogeneous soil conditions compared with different methods (t = 0.01D, v_s = 0.25-0.35).

Figure 9 illustrates a similar relationship between $K_{LR}/(E_sD^2)$ and both (L_p/D) and $\ln(E_{eq}/E_s)$ in the 3-D context. In Figure 9b, it is evident that the values of $K_{LR}/(E_sD^2)$ decrease with increasing L_p/D, and the values from the present study at $L_p/D = 2$ align well with the results of Shadlou et al. [20] for rigid pile conditions, as presented in Tables 1 and 2. Furthermore, $K_{LR}/(E_sD^2)$ from the present study becomes insensitive to L_p/D as L_p/D increases. In Figure 9c, the results from the present study, where $L_p/D \geq 6$, better align with the equations from Shadlou et al. [20] for flexible piles, indicating that $K_{LR}/(E_sD^2)$ exhibits behavior characteristic of flexible piles in this regime. A similar phenomenon has been observed in Figure 10, where $K_R/(E_sD^3)$ versus $(L_p/D, \ln(E_{eq}/E_s))$ in the 3-D context

were analyzed, further emphasizing the importance of considering these parameters for accurate predictions in laterally loaded foundation analysis.

The observations made in Figures 8–10 highlight the limitations of traditional methods in covering all calculating conditions for foundations with $D \geq 2$ m and $2 \leq L_p/D \leq 10$ in heterogeneous soil conditions. It becomes evident that the functions of $K_L/(E_sD)$, $K_{LR}/(E_sD^2)$, and $K_R/(E_sD^3)$ should indeed be expressed as functions of E_{eq}/E_s and L_p/D in heterogeneous soil conditions, necessitating the development of more accurate equations that account for both of these parameters. Moreover, the threshold zones for long flexible piles and short rigid piles in heterogeneous soil conditions differ from those in inhomogeneous and linearly inhomogeneous soils, underlining the importance of considering specific soil characteristics when analyzing foundation behavior.

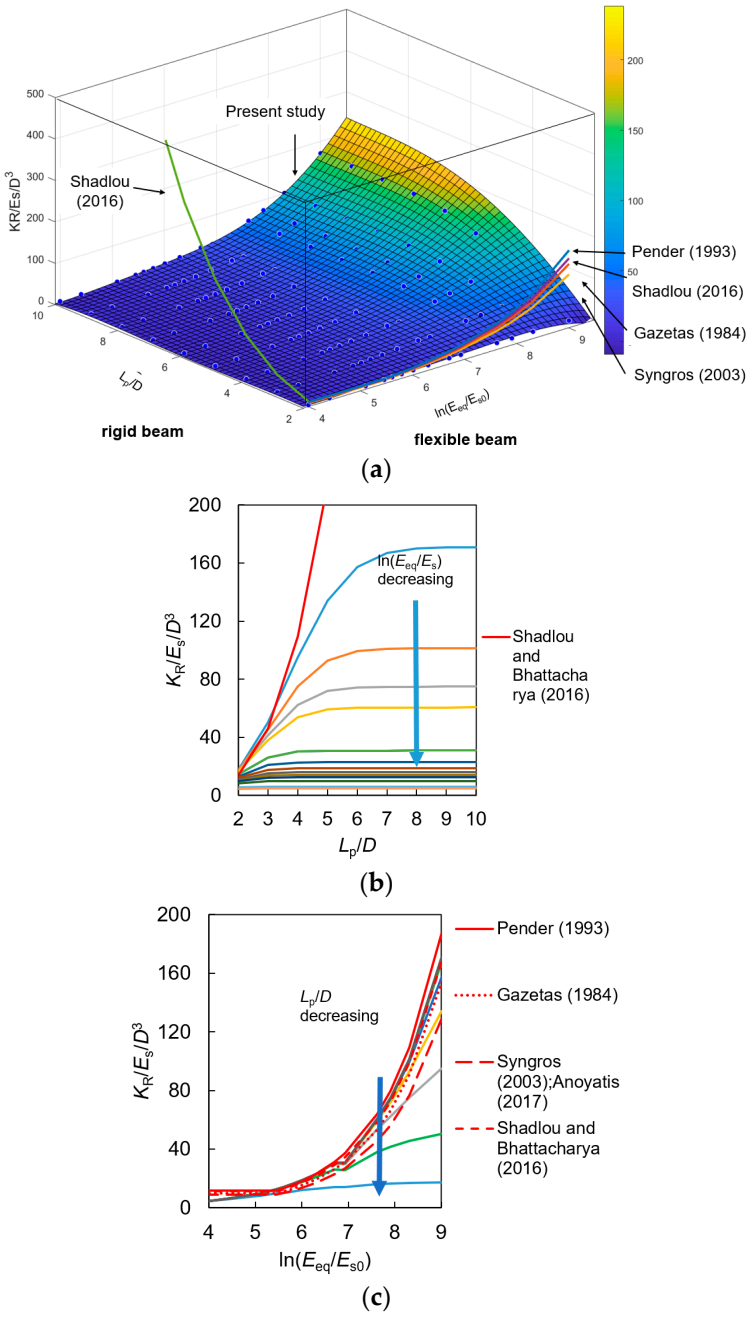

Figure 10. The results of $K_R/(E_sD^3)$ at (**a**) 3-D, (**b**) L_p/D and (**c**) $\ln(E_{eq}/E_s)$ version in heterogeneous soil conditions compared with different methods ($t = 0.01D$, $v_s = 0.30$).

Heterogeneous soil conditions (α = 0.25 and 0.75). Additionally, a similar phenomenon observed in $K_L/(E_sD)$, $K_{LR}/(E_sD^2)$, and $K_R/(E_sD^3)$ versus (L_p/D, $\ln(E_{eq}/E_s)$) when α = 0.25 and 0.75 in the 3-D context further emphasizes the need for more accurate equations that can account for a wider range of scenarios without relying on the critical length parameter. This suggests the importance of developing equations that consider both the relative stiffness of the pile and soil and the slenderness ratio in future studies.

3.2. Parameter Analysis

The effect of materials and thickness. Figures 11 and 12 provide valuable insights into the behavior of foundations in heterogeneous soil conditions with varying materials. In Figure 11, which considers different materials (steel piles with $t = 0.01D$ and concrete piles with $0.1D$) and α = 0.75, the results for $K_L/(E_sD)$ show that the difference between these materials is within 3%. This suggests that using the function E_{eq}/E_s is an effective way to account for different materials of hollow piles when analyzing the head stiffness of foundations in heterogeneous soil conditions. Similarly, in Figure 12, which focuses on concrete piles with varying wall thicknesses ($t = 0.1D$ and $0.15D$) and α = 0.25, v_s = 0.30, the results for $K_L/(E_sD)$ also indicate that the difference between these material variations is within 3%. This further supports the notion that the function E_{eq}/E_s is a robust approach for considering material variations in the analysis of foundation behavior in heterogeneous soil conditions. These findings suggest that, compared with Poulos and Davis [14] and Aissa et al. [21], the function E_{eq}/E_s can efficiently incorporate different materials in the analysis, simplifying the modeling process while maintaining accuracy in predicting the behavior of foundations with varying materials.

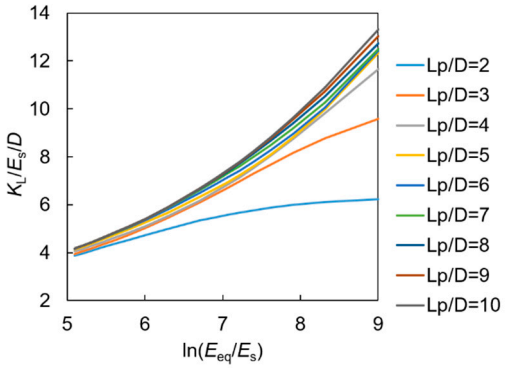

Figure 11. $K_L/(E_{s0}D)$ in heterogeneous soil conditions (α = 0.75, t = 0.1D, E_p = 30 Gpa and 210 Gpa, v_s = 0.30).

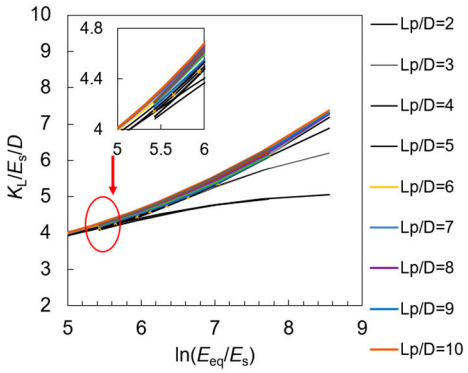

Figure 12. $K_L/(E_sD)$ in heterogeneous soil conditions compared with different methods (α = 0.25, $t = 0.05D$ and $0.15D$, concrete material, v_s = 0.30).

The effect of Poisson's ratio. The consideration of Poisson's ratio in the analysis of $K_L/(E_sD)$, $K_{LR}/(E_sD^2)$, and $K_R/(E_sD^3)$ is relatively important. In previous research, the

effect of Poisson's ratio on $K_L/(E_sD)$, $K_{LR}/(E_sD^2)$, and $K_R/(E_sD^3)$ is commonly neglected in some studies. Randolph [13] considered the effect by $f(v_s) = (1 + 0.75\ v_s)/(1+ v_s)$; Shadlou and Bhattacharya [20] gave the function $f(\nu_s) = 1 + |\nu_s - 0.25|$; Jabli et al. [52] presented solutions for stiffness of suction caissons having rigid skirted for $0.5 < L/D < 2$ in three types of ground profiles with $f(\nu_s) = 1 + 0.6|\nu_s - 0.25|$ and by $f(v_s) = 1.1(0.096L_p/D + 0.6)v_s^2 - 0.7v_s + 1.06$. In this paper, the effect of Poisson's ratio is observed, and it's noted that the effect is influenced by various factors, including $\ln(E_{eq}/E_s)$, L_p/D, and α. Comparing the values obtained for different Poisson's ratios (v_s = 0.2 to v_s = 0.45) with those for v_s = 0.30 under the same pile and soil conditions, it's observed that the error ranges from −2% to 14%. This suggests that accounting for varying Poisson's ratios in soils is essential for accurate analysis. Compared with Randolph [13] and Jabli et al. [52], a more efficient way is proposed to take into account different Poisson's ratios in soils, and the following equation can be used:

$$f^{(1)}(\nu_s) = f^{(2)}(\nu_s) = (-0.7146\alpha + 2.837)\nu_s^2 - (-0.2666\alpha + 1.4381)\nu_s + 1.17 \quad (12)$$

$$f^{(3)}(\nu_s) = 1 + 0.4|\nu_s - 0.3| \quad (13)$$

The proposed equation for considering different Poisson's ratios (v_s) in soils has limited the errors in $K_L/(E_sD)$, $K_{LR}/(E_sD^2)$, and $K_R/(E_sD^3)$ to a range of −1.5% to 5% across all cases in Table 3. Figure 13 gives an example of the modification effect of Equations (12) and (13) for $K_L/(E_sD)$ in different conditions (α = 0 to 1, concrete and steel material), where the values of K_L at v_s = 0.2 to 0.45 were divided by the value of K_L when v_s = 0.3. results show that the values are in the range of 0.985 to 1.035, and the average values are nearly equal to 1.0. This suggests that the equation effectively accounts for variations in Poisson's ratio and provides accurate predictions for the behavior of foundations under different soil conditions.

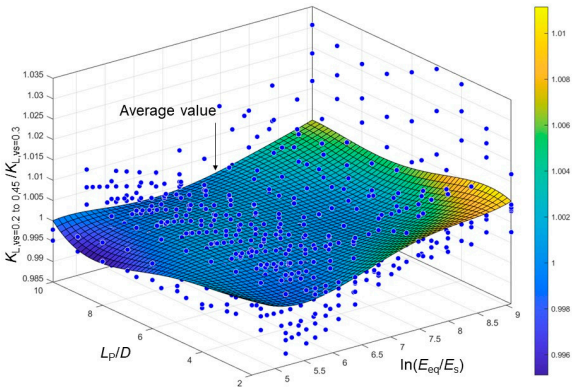

Figure 13. $K_{L,vs=0.2\ to\ 0.45}/K_{L,vs=0.3}$ in different conditions (α = 0 to 1, concrete and steel material v_s = 0.2 to 0.45).

3.3. The Equations of Stiffness of Pile-Head Springs

From Section 3.1, the dimensionless function of the stiffness of pile-head springs, $g^{(n)}$, can be described by a serial of polynomial equations containing $\ln(E_{eq}/E_{s0})$ and L_p/D:

$$g^{(n)}\left(\ln\left(\frac{E_{eq}}{E_{s0}}\right), \frac{L_p}{D}\right) = \sum_{i=0}^{i=3}\sum_{j=0}^{j=4} P_{ij}^{(n)}\left(\ln\left(\frac{E_{eq}}{E_{s0}}\right)\right)^i\left(\frac{L_p}{D}\right)^j \quad (14)$$

where $g^{(n)}$ is the polynomial function related to $K_L/E_{s0}D$, $K_{LR}/E_{s0}D^2$ and $K_R/E_{s0}D^3$ at v_s = 0.3, respectively; n = 1, 2, 3, $g^{(1)}$ is the constant of K_L, $g^{(2)}$ is the constant of K_{LR}, $g^{(3)}$ is the constant of K_R; P_{ij} is the dimensionless constant (i = 0, 1, 2, 3; j = 0, 1, 2, 3, 4); the value of $P^{(1)}{}_{ij}$ is shown in Table 4, the value of $P^{(2)}{}_{ij}$ is shown in Table 5, the value of $P^{(3)}{}_{ij}$ is shown in Table 6.

Table 4. The content of K_L.

Value	P_{00}	P_{10}	P_{01}	P_{20}	P_{11}	P_{02}	P_{30}	P_{21}	P_{12}	P_{03}	P_{31}	P_{22}	P_{13}	P_{04}
$\alpha = 0$	−0.1946	1.585	0.5968	−0.1631	−0.4379	0.06025	0	0.07794	−0.01022	−0.001649	0	−0.005156	0.003405	−0.0006621
$\alpha = 0.25$	0.3576	0.8363	−0.1893	−0.01239	−0.01615	0.06096	−0.01037	0.02333	−0.02733	0.003275	0.003736	−0.006168	0.004877	−0.001146
$\alpha = 0.5$	1.387	0.1003	0.1399	0.1291	−0.1217	0.03236	−0.02091	0.04254	−0.03505	0.01073	0.004781	−0.008981	0.007158	−0.002031
$\alpha = 0.75$	−0.6245	0.5882	0.7791	0.135	−0.4054	0.06082	−0.02838	0.07991	−0.04049	0.01065	0.006437	−0.01417	0.01121	−0.003105
$\alpha = 1.0$	−0.828	0.7034	0.1463	0.1117	−0.2019	0.1179	−0.03042	0.07791	−0.08425	0.02335	0.008512	−0.01638	0.015	−0.004651

Table 5. The content of K_{LR}.

Value	P_{00}	P_{10}	P_{01}	P_{20}	P_{11}	P_{02}	P_{30}	P_{21}	P_{12}	P_{03}	P_{31}	P_{22}	P_{13}	P_{04}
$\alpha = 0$	−12.96	7.616	0.1802	−1.802	−0.5758	0.1998	0.1437	0.2000	−0.06428	−0.00767	−0.03409	0.0266	−0.01054	0.002288
$\alpha = 0.25$	−9.391	5.391	0.8606	−1.424	−0.5084	−0.04152	0.133	0.1489	−0.0149	0.003804	−0.03747	0.0351	−0.01815	0.003377
$\alpha = 0.5$	−3.061	3.251	−0.6617	−1.265	−0.1393	0.1574	0.1443	0.1388	−0.05027	−0.01146	−0.04832	0.05271	−0.02807	0.006426
$\alpha = 0.75$	−0.6676	4.592	−3.002	−1.937	0.2958	0.4112	0.2146	0.2178	−0.184	0.007226	−0.07174	0.08561	−0.04499	0.01009
$\alpha = 1.0$	11.21	−0.8236	−1.624	−1.192	0.003626	0.1521	0.1971	0.216	−0.09182	−0.005945	−0.08304	0.1031	−0.06253	0.01531

Table 6. The content of K_R.

Value	P_{00}	P_{10}	P_{01}	P_{20}	P_{11}	P_{02}	P_{30}	P_{21}	P_{12}	P_{03}	P_{31}	P_{22}	P_{13}	P_{04}
$\alpha = 0$	131.2	−82.5	−15.48	17.05	14.32	−2.878	−1.153	−3.607	0.9585	0.03846	0.3045	−0.09629	−0.008377	0.002295
$\alpha = 0.25$	82.54	−56.65	−13.35	13.38	10.44	−0.9526	−1.048	−3.021	0.8748	−0.1454	0.319	−0.156	0.0314	0.001307
$\alpha = 0.5$	76.44	−58.59	−10.91	14.67	11.83	−2.367	−1.209	−3.7	1.362	−0.1506	0.4116	−0.249	0.06592	−0.005961
$\alpha = 0.75$	144.1	−102.1	−21.31	23.48	21.57	−5.23	−1.804	−6.166	2.572	−0.2827	0.6233	−0.4138	0.1193	−0.01369
$\alpha = 1.0$	63.22	−67.89	−17.9	19.33	19.84	−4.724	−1.71	−6.207	2.814	−0.4226	0.6904	−0.5235	0.1853	−0.0248

From Section 3.2, the effect of Poisson's ratio is given by Equations (12) and (13). Put Equations (12) and (13) into Equation (14), the semi-experimental equations of K_L, $K_{LR,}$ and K_R considering the effects of Poisson's ratio are given as:

$$\frac{K_L}{E_{s0}D} = g^{(1)}f^{(1)}(\nu_s) \tag{15}$$

$$\frac{K_{LR}}{E_{s0}D^2} = g^{(2)}f^{(2)}(\nu_s) \tag{16}$$

$$\frac{K_R}{E_{s0}D^3} = g^{(3)}f^{(3)}(\nu_s) \tag{17}$$

The polynomial equations proposed in Equations (15)–(17) exhibit a strong fit with the outcomes obtained through the energy-based variational method in Table 3, with a coefficient of determination (R^2) exceeding 0.997.

4. Application of the Methodology

4.1. The Lateral Deflection and Rotation of Caissons for Serviceability Limit State Calculations

In the design process, caissons cannot be decidedly classified as slender or rigid beams. By using Equations (15)–(17), the head stiffness of the caissons was given, and the values can be put into Equation (18) to predict the lateral deflection and rotation at the caisson's head. The results are given in Table 7.

$$\begin{aligned} w &= \frac{K_R}{K_L K_R - K_{LR}^2}F_a - \frac{K_{LR}}{K_L K_R - K_{LR}^2}M_a \\ \theta &= -\frac{K_{LR}}{K_L K_R - K_{LR}^2}F_a + \frac{K_L}{K_L K_R - K_{LR}^2}M_a \end{aligned} \tag{18}$$

Table 7. Detail of parameters in studies.

F_a (kN)	$M_a/F_a/L_p$ (kNm)	D	L_p	t	E_s	v_s	I_p	$\ln(E_P/E_{S0})$	L_p/D
2000	0 to 1	5	12	0.4	60	0.25	15.40	5.5257	2.4
		2					0.68	5.5257	6

Table 7 and Figure 14 present the head stiffness of the caissons obtained from Equations (15)–(17) and Tables 4–6. Results show that these values differ significantly from those provided by Shadlou et al. [20], who categorized caissons as either rigid or flexible beams. This suggests that the proposed method in this paper takes into account the caissons' behavior more accurately by not categorizing them as strictly rigid or flexible. Table 8 outlines the parameters for comparing lateral deflection and rotation between the method in this paper, Shadlou [20], and FEM analysis performed by ABAQUS [53]. The relative parameters are presented in Table 8, where different $M_a/F_a/L_p$ were covered. In the FEM, half models were built, both the method in this paper and the FEM analysis use consistent characteristics of the caisson and soil properties, grid size, boundary conditions, and method of force application, which is essential for a meaningful comparison. However, the method in this paper employs the Timoshenko beam to construct the caisson, whereas FEM analysis employs the solid element.

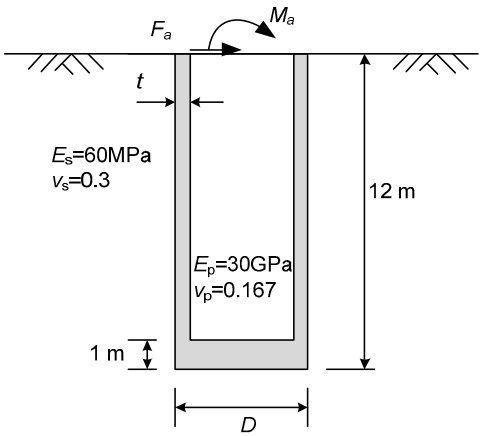

Figure 14. A laterally loaded caisson.

Table 8. The values of K_L, K_{LR} and K_R.

Parameters	Present Study		Shadlou et al. [20] (Rigid)		Shadlou [20] (Flexible)
	***D* = 2 m**	***D* = 5 m**	***D* = 2 m**	***D* = 5 m**	***D* = 2 m**
K_L	1244	497	1652	1166	486
K_{LR}	−7310	−1208	−9992	−6677	−1141
K_R	78,716	6606	110,426	69,840	4879

Figure 15a illustrates a comparison of lateral deflection errors between this study, FEM, and Shadlou et al. [20] for different values of L_p/D, specifically L_p/D = 2.4 and L_p/D = 6. The errors in lateral deflection range from 8% to 12% for L_p/D = 2.4 and from −2% to 6% for L_p/D = 6 when compared to FEA results. In contrast, the errors from Shadlou et al. [20] and an unspecified FEM show significantly higher deviations, with errors ranging from −26% to −21% for L_p/D = 2.4 and −54% to 36% for L_p/D = 6. Similarly, Figure 15b presents a comparison of the rotation errors obtained from the head stiffness equations (Equations (15)–(17)) in this study with FEM results and those from Shadlou et al. [20]. The rotation errors from this study are found to be more consistent with FEM results when compared to those from Shadlou et al. [20].

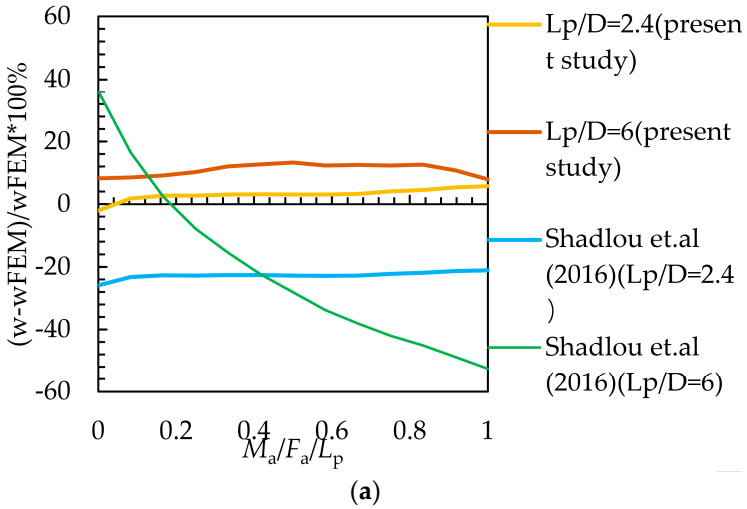

(**a**)

Figure 15. *Cont.*

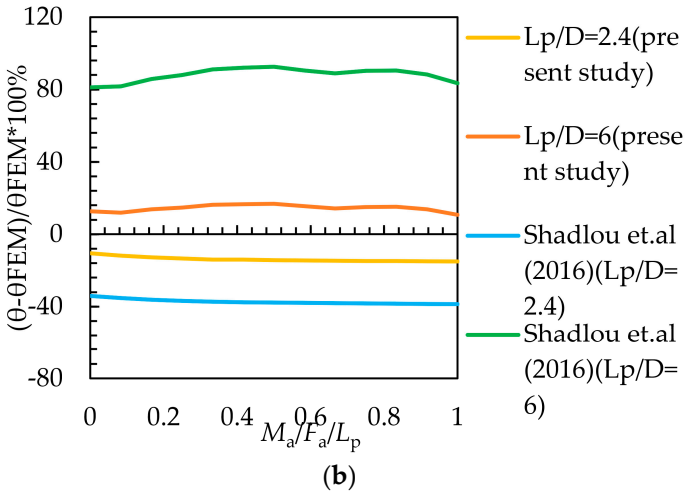

(**b**)

Figure 15. The error of (**a**) the lateral deflection and (**b**) the rotation from different methods with L_p/D = 2.4 and L_p/D = 6 (w_{FEM} is the head lateral deflection of caissons from ABAQUS, θ_{FEM} is the head rotation of caissons from ABAQUS).

Therefore, in the case of a semi-rigid caisson, the prediction of head deflection and rotation under static loading conditions is significantly contingent on the accurate determination of its head stiffness. Hence, there is a clear imperative to develop a more precise method for forecasting head stiffness.

4.2. The Natural Frequency of OWT Considering the SSI Effect

Three cases from Belwind [54], Walney [36] and Kentish Flats Offshore Wind Farm [54] were adopted to verify the accuracy of Equations (15)–(17) in predicting the natural frequencies of Offshore Wind Turbine (OWT) models while considering the Soil-Structure Interaction (SSI) effect. The relative parameters of the OWT system are presented in Figure 16 and detailed in Table 9. For the modification of the OWT system, FEM was conducted using ABAQUS [53], and a concentrated mass block was placed on top of a series of Timoshenko beams. To account for the monopile-soil interaction, three types of springs with initial stiffness values of K_L, K_{LR}, and K_R, which were calculated using Equations (15)–(17), were used to account for the SSI effect.

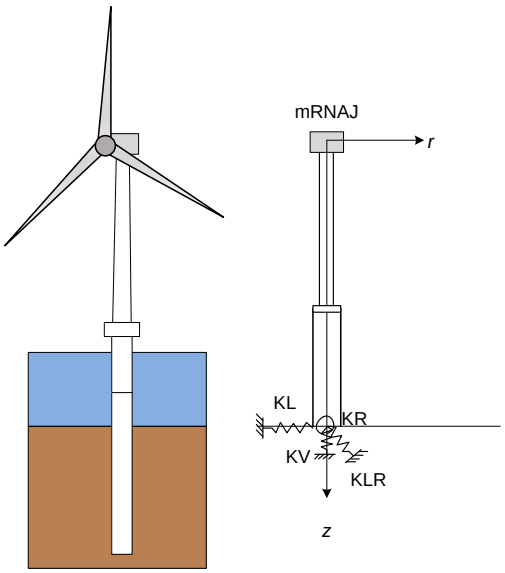

Figure 16. An OWT model considering the SSI effect.

Table 9. The relative parameters of OWT system.

Parameters		Belwind	Walney [36]	Kentish Flats Offshore Wind Farm
Rated power (MW)		3	3.6	-
Mass of rotor-nacelle assembly (m_{RNA}) (kg)		130,800	234,500	132,000
Tower height		53	67.3	60.06
Tower bottom diameter (m)		4.3	5	4.45
Tower top diameter (m)		2.3	3	2.3
Tower wall bottom thickness (mm)		28	41	26
Tower wall top thickness (mm)		28	41	15
Tower Young's modulus (GPa)		210	210	210
Tower density (kg/m^3)		7860	7860	7960
Transfer piece diameter (m)		5	6	4.3
Platform height above mudline (m)		37	37.3	14.94
Monopile diameter (D) (m)		5	6	4.3
Monopile thickness (mm)		60	80	45
Monopile length (m)		35	23.5	29.5
Monopile young's modulus (GPa)		210	210	210
Soil type		2	2	1
E_{s0} (Mpa)		15	30	52
v_s		0.3	0.25	0.4
α		1	1	0
From previous studies (Laszlo, [54]; Gupat et al. [36])	lateral stiffness of foundation (GN/m^3)	1.02	1.53	0.82
	cross stiffness of foundation, K_{LR} (GN)	−7.59	−13.88	−5.42
	Rocking stiffness of foundation, K_R (GN/rad)	91.93	205.72	58.77
From this paper	lateral stiffness of foundation, K_L (GN/m^3)	0.626	1.22	1.04
	cross stiffness of foundation, K_{LR} (GN)	−5.74	−12.94	−5.72
	Rocking stiffness of foundation, K_R (GN/rad)	89.24	205.26	66.69

From Table 9, it is observed that in the second case, where the critical length of the pile aligns more closely with a slender pile (as indicated in Table 1), the results of K_L, K_{LR}, and K_R closely match those from the reference [54]. Conversely, in the first and the third cases, where the classification of the pile as slender or rigid is less clear based on Tables 1 and 2, the results from the first case are lower than those expected for a typical rigid pile according to the reference [54], on the other hand, the results from the third case are higher than those expected for a typical flexible pile according to the reference [54].

The proposed method in this study has also been verified to enhance the accuracy of natural frequency predictions for OWT models considering the SSI effect. The natural frequencies of wind turbine structures, after accounting for the SSI effect, are provided in Table 10. Among the studied cases, the first natural frequency, as evaluated by both the references and this study, closely aligns with field testing results in the rotor-stop condition. However, discrepancies become more apparent in higher natural frequencies, with the largest error reaching 13%. This underscores the need for a more accurate equation for calculating dimensionless head stiffness, particularly when dealing with high-order self-resonant frequency calculations.

Table 10. Influence of spring stiffness on the natural frequencies of the elastically supported immersed beam with eccentricity.

Offshore Wind Farm	Mode	Measured Frequency	Frequency (ABAQUS)		Error (%)
			From Previous Studies	From This Paper	
Belwind	1	0.372	0.364	0.365	−0.27
	2	-	0.379	0.383	−1.04
	3	-	5.083	5.006	1.54
	4	-	6.279	6.483	−3.15
	5	-	15.827	15.720	0.68
	10	-	88.20	88.09	0.12
	18	-	303.26	300.36	0.97
Walney	1	0.350	0.337	0.337	0.00
	2	-	0.427	0.404	5.82
	4	-	10.876	10.195	6.68
	5	-	10.887	10.876	0.10
	10	-	50.187	49.823	0.73
	20	-	163.28	162.83	0.28
Kentish Flats Offshore Wind Farm	1	0.339	0.343	0.342	0.00
	3	-	7.3693	6.736	9.40
	5	-	13.395	11.954	12.05
	7	-	35.449	31.339	13.11
	10	-	79.674	73.455	8.47
	18	-	316.35	300.31	5.34

5. Conclusions

This study focuses on developing a precise method for calculating the head static stiffness of semi-rigid piles, without the need to consider the critical length, a parameter commonly used in traditional approaches. To achieve this objective, an extensive analysis comprising nearly twenty thousand cases was conducted using the energy-based variational method with Timoshenko beam theory. These cases encompassed a wide range of scenarios, including steel pipe piles and concrete caissons with diameters ranging from 2 m to 10 m, slenderness ratios between 2 and 10, and various soil types represented by the parameter α (ranging from 0 to 1) with a wide range of elastic moduli (E_s) from 2 Mpa to 300 Mpa and Poisson's ratios (v_s) spanning 0.2 to 0.45.

The results demonstrate a limitation of traditional methods, as they fail to cover the full spectrum of foundation conditions within the aforementioned range. In contrast, the polynomial equations proposed in this paper exhibit a strong fit with the outcomes obtained through the energy-based variational method, with a coefficient of determination (R^2) exceeding 0.997.

In practical applications, the method introduced in this study offers a distinct advantage. It enables engineers to achieve accurate results for head deflection and rotation of foundations under static loading conditions without the need for FDM or FEM software. This research also contributes to a more precise and accessible method for calculating foundation behavior, with potential applications in the analysis of high-order self-resonant frequencies in Offshore Wind Turbine (OWT) systems.

Notably, while these equations are applicable to a wide range of soil types and foundation scenarios, caution should be exercised when applying them to unique or unconventional cases without the aforementioned range, such as monopiles embedded in rocks.

Author Contributions: Conceptualization, W.L. and X.L.; methodology, X.L.; software, Q.Y.; validation, X.L., W.L. and M.Z.; formal analysis, M.Z.; investigation, X.L.; resources, X.L.; data curation, T.W.; writing—original draft preparation, W.L.; writing—review and editing, X.L.; visualization, T.W.; supervision, Q.Y.; project administration, X.L.; funding acquisition, X.L. All authors have read and agreed to the published version of the manuscript.

Funding: This research was funded by the National Natural Science Foundation of China [52201324] and the Natural Science Foundation of the Jiangsu Higher Education Institution of China [22KJB560015].

Data Availability Statement: The data presented in this study are available on request from the corresponding author.

Acknowledgments: The authors would like to thank the National Natural Science Foundation of China, and the Natural Science Foundation of the Jiangsu Higher Education Institution of China. The authors are grateful for their support.

Conflicts of Interest: The authors declare no conflict of interest.

Notation

The following symbols are used in this paper:

D	the outer diameter of caisson
dw/dz	the rotation of the beam section
E_{eq}	the equivalent Young's modulus of the beam
E_{p}	the Young's modulus of the beam
E_{si}	the elastic modulus of the ith layer of soil
E_{s0}	the initial value of soil elastic modulus
$\boldsymbol{F}_{\mathrm{a}}$	the lateral force at the head of beam
I_{p}	the second moment of inertia of cross-section
K_{L}	lateral stiffness
K_{R}	rocking stiffness
K_{LR}	cross-coupling stiffness
L_{p}	the embedment depth of beam
m_{RNA}	mass of rotor-nacelle assembly (kg)
M_{a}	the moment at the head of beam
R^2	a coefficient of determination
r_{p}	the radius of the beam
t	the wall thickness of beam
u_z	the vertical displacement
w	the lateral displacement of the beam central line
α	the index of the function
γ	the relative stiffness of the pile and soil
Ω	the soil domain that participates in the structure-soil interaction
ϕ	the shear rotation of the plane section
κ	the shear correction factor
σ_{pq}	the stress in soil domain
ε_{pq}	the strain in soil domain
λ_{si}, G_{si}	the Lame's constants of the ith layer of the multilayered continuum
v_{si}	the Poisson's ratio of the ith layer of soil
ϕ_r	dimensionless decay functions of the displacement components in the r-directions
ϕ_θ	dimensionless decay functions of the displacement components in the θ-directions
ϕ_z	dimensionless decay functions of the displacement components in the z-directions

Appendix A

For the beam at $z \leq L_{\mathrm{p}}$, the governing differential equations of $w(z)$ and $\phi(z)$ are coupled, and these equations are given by:

$$\kappa G_p A_p \left(\frac{d^2 w}{dz^2} - \frac{d\phi}{dz} \right) + 2t \frac{d^2 w}{dz^2} + k_1 \frac{d\phi}{dz} - kw = 0 \tag{A1}$$

and

$$E_p I_p \frac{d^2 \phi}{dz^2} + \kappa G_p A_p \left(\frac{dw}{dz} - \phi \right) - k_3 \phi - k_1 \frac{dw}{dz} + 2t_4 \frac{d^2 \phi}{dz^2} = 0 \tag{A2}$$

where $\frac{\pi}{2}\int_{rp}^{\infty} Gs(\phi_r^2+\phi_\theta^2)rdrdr = t$, $\pi\int_{rp}^{\infty}\{G_s r_p\frac{d\phi_z}{dr}\phi_r + G_s\frac{r_p}{r}\phi_z\phi_\theta - \lambda_s r_p\phi_z\frac{d\phi_r}{dr} - \lambda_s r_p\phi_z\frac{\phi_r-\phi_\theta}{r}\}$
$rdr = k_1$, $\pi\int_{rp}^{\infty}\{(\lambda_s+2G_s)(\frac{d\phi_r}{dr})^2 + 2\lambda_s\frac{\phi_r-\phi_\theta}{r}\frac{d\phi_r}{dr} + (\lambda_s+2G_s)(\frac{\phi_r-\phi_\theta}{r})^2 + G_s(\frac{\phi_r-\phi_\theta}{r}+\frac{d\phi_\theta}{dr})^2\}$
$rdr = k$, $\pi\int_{rp}^{\infty}\{G_s\{\frac{\phi_z}{r}\phi_\theta + \frac{d\phi_z}{dr}\phi_r\}r_p rdr = k_2$, $\pi\int_{rp}^{\infty}\{[G_s\frac{d\phi_z}{dr}\frac{d\phi_z}{dr} + G_s\frac{\phi_z}{r}\frac{\phi_z}{r}]r_p^2 rdr = k_3$,
$\frac{\pi}{2}\int_{rp}^{\infty}(\lambda_s+2G_s)\phi_z^2 r_p^2 rdr = t_4$.

Appendix B

The boundary conditions at the end of the foundation are calculated by:
At the pile head:
(1) F_a = *constant*, $\theta_0 = 0$

$$\begin{aligned}&\kappa G_p A_p\left(\tfrac{dw}{dz}-\phi\right)+k_2\phi+2t\tfrac{dw}{dz} = -F_a\\ &\tfrac{dw}{dz} = 0\end{aligned} \tag{A3}$$

where

$$\left[\begin{array}{l}\frac{(-\kappa G_pA_p+k_2)(E_pI_p+2t_4)(\kappa G_pA_p+2t)}{(\kappa G_pA_p-k_1)(\kappa G_pA_p+k_3)}\Phi_1''' + \left(-\frac{(-\kappa G_pA_p+k_2)(E_pI_p+2t_4)k}{(\kappa G_pA_p+k_3)(\kappa G_pA_p-k_1)} + \frac{(-\kappa G_pA_p+k_2)(\kappa G_pA_p-k_1)}{(\kappa G_pA_p+k_3)} + (\kappa G_pA_p+2t)\right)\Phi_1'\\ \frac{(-\kappa G_pA_p+k_2)(E_pI_p+2t_4)(\kappa G_pA_p+2t)}{(\kappa G_pA_p-k_1)(\kappa G_pA_p+k_3)}\Phi_2''' + \left(-\frac{(-\kappa G_pA_p+k_2)(E_pI_p+2t_4)k}{(\kappa G_pA_p+k_3)(\kappa G_pA_p-k_1)} + \frac{(-\kappa G_pA_p+k_2)(\kappa G_pA_p-k_1)}{(\kappa G_pA_p+k_3)} + (\kappa G_pA_p+2t)\right)\Phi_2'\\ \frac{(-\kappa G_pA_p+k_2)(E_pI_p+2t_4)(\kappa G_pA_p+2t)}{(\kappa G_pA_p-k_1)(\kappa G_pA_p+k_3)}\Phi_3''' + \left(-\frac{(-\kappa G_pA_p+k_2)(E_pI_p+2t_4)k}{(\kappa G_pA_p+k_3)(\kappa G_pA_p-k_1)} + \frac{(-\kappa G_pA_p+k_2)(\kappa G_pA_p-k_1)}{(\kappa G_pA_p+k_3)} + (\kappa G_pA_p+2t)\right)\Phi_3'\\ \frac{(-\kappa G_pA_p+k_2)(E_pI_p+2t_4)(\kappa G_pA_p+2t)}{(\kappa G_pA_p-k_1)(\kappa G_pA_p+k_3)}\Phi_4''' + \left(-\frac{(-\kappa G_pA_p+k_2)(E_pI_p+2t_4)k}{(\kappa G_pA_p+k_3)(\kappa G_pA_p-k_1)} + \frac{(-\kappa G_pA_p+k_2)(\kappa G_pA_p-k_1)}{(\kappa G_pA_p+k_3)} + (\kappa G_pA_p+2t)\right)\Phi_4'\end{array}\right]^T_{z=0}$$

$$\begin{bmatrix}C_1\\C_2\\C_3\\C_4\end{bmatrix}^{(1)}_{z=0} = -F_a \text{ and } \begin{bmatrix}\Phi_1'\\\Phi_2'\\\Phi_3'\\\Phi_4'\end{bmatrix}^T_{z=0}\begin{bmatrix}C_1\\C_2\\C_3\\C_4\end{bmatrix}^{(1)}_{z=0} = 0.$$

(2) w_0 = *constant*, $\theta_0 = 0$

$$\begin{aligned}&w_0 = 1\\ &\tfrac{dw}{dz} = 0\end{aligned} \tag{A4}$$

where $\begin{bmatrix}\Phi_1\\\Phi_2\\\Phi_3\\\Phi_4\end{bmatrix}^T_{z=0}\begin{bmatrix}C_1\\C_2\\C_3\\C_4\end{bmatrix}^{(1)}_{z=0} = 1$ and $\begin{bmatrix}\Phi_1'\\\Phi_1'\\\Phi_3'\\\Phi_4'\end{bmatrix}^T_{z=0}\begin{bmatrix}C_1\\C_2\\C_3\\C_4\end{bmatrix}^{(1)}_{z=0} = 0.$

(3) M_a = *constant*, $w_0 = 0$

$$\begin{aligned}&w_0 = 0\\ &E_pI_p\tfrac{d\phi}{dz} + (-k_1+k_2)w + 2t_4\tfrac{d\phi}{dz} = M_a\end{aligned} \tag{A5}$$

where $\begin{bmatrix}\Phi_1\\ \Phi_2\\ \Phi_3\\ \Phi_4\end{bmatrix}^T_{z=0}\begin{bmatrix}C_1\\ C_2\\ C_3\\ C_4\end{bmatrix}^{(1)}_{z=0} = 0$ and

$$\begin{bmatrix} \frac{(E_pI_p+2t_4)}{(\kappa G_pA_p-k_1)}(\kappa G_pA_p+2t)\Phi_1'' + \left(-\frac{k(E_pI_p+2t_4)}{(\kappa G_pA_p-k_1)}+(-k_1+k_2)\right)\Phi_1 \\ \frac{(E_pI_p+2t_4)}{(\kappa G_pA_p-k_1)}(\kappa G_pA_p+2t)\Phi_2'' + \left(-\frac{k(E_pI_p+2t_4)}{(\kappa G_pA_p-k_1)}+(-k_1+k_2)\right)\Phi_2 \\ \frac{(E_pI_p+2t_4)}{(\kappa G_pA_p-k_1)}(\kappa G_pA_p-P+2t)\Phi_3'' + \left(-\frac{k(E_pI_p+2t_4)}{(\kappa G_pA_p-k_1)}+(-k_1+k_2)\right)\Phi_3 \\ \frac{(E_pI_p+2t_4)}{(\kappa G_pA_p-k_1)}(\kappa G_pA_p-P+2t)\Phi_4'' + \left(-\frac{k(E_pI_p+2t_4)}{(\kappa G_pA_p-k_1)}+(-k_1+k_2)\right)\Phi_4 \end{bmatrix}^T_{z=0}\begin{bmatrix}C_1\\ C_2\\ C_3\\ C_4\end{bmatrix}^{(1)}_{z=0} = M_a.$$

The boundary conditions for the ith layer (i = 1, 2, 3, …, n) of the beam at $z = H_i < L_p$ are calculated by:

$$\begin{aligned} &w_{i,z=Hi} = w_{i+1,z=Hi}\\ &\tfrac{dw}{dz}_{i,z=Hi} = \tfrac{dw}{dz}_{i+1,z=Hi}\\ &\left\{\kappa G_pA_p\left(\tfrac{dw}{dz}-\phi\right)+\{k_2\phi+2t\tfrac{dw}{dz}\}\right\}_{i,z=Hi} = \left\{\kappa G_pA_p\left(\tfrac{dw}{dz}-\phi\right)+k_2\phi+2t\tfrac{dw}{dz}\right\}_{i+1,z=Hi}\\ &\left\{E_pI_p\tfrac{d\phi}{dz}+(-k_1+k_2)w+2t_4\tfrac{d\phi}{dz}\right\}_{i,z=Hi} = \left\{E_pI_p\tfrac{d\phi}{dz}+(-k_1+k_2)w+2t_4\tfrac{d\phi}{dz}\right\}_{i+1,z=Hi}\end{aligned} \quad (A6)$$

where

$$\begin{bmatrix} \Phi_1 & \Phi_2 & \Phi_3 & \Phi_4 \\ \Phi_1' & \Phi_2' & \Phi_3' & \Phi_4' \\ \frac{(E_pI_p+2t_4)(\kappa G_pA_p+2t)}{(\kappa G_pA_p-k_1)(\kappa G_pA_p+k_3)}\Phi_1''' + \left(-\frac{(E_pI_p+2t_4)k}{(\kappa G_pA_p+k_3)(\kappa G_pA_p-k_1)}+\frac{(\kappa G_pA_p-k_1)}{(\kappa G_pA_p+k_3)}+\frac{(\kappa G_pA_p+2t)}{(-\kappa G_pA_p+k_2)}\right)\Phi_1' & . & . & . \\ \frac{(E_pI_p+2t_4)}{(\kappa G_pA_p-k_1)}(\kappa G_pA_p+2t)\Phi_1'' + \left(-\frac{(E_pI_p+2t_4)}{(\kappa G_pA_p-k_1)}k+(-k_1+k_2)\right)\Phi_1 & . & . & . \end{bmatrix}^{(i)}_{z=z_i}\begin{bmatrix}C_1\\ C_2\\ C_3\\ C_4\end{bmatrix}^{(i)}_{z=z_i} =$$

$$\begin{bmatrix} \Phi_1 & \Phi_2 & \Phi_3 & \Phi_4 \\ \Phi_1' & \Phi_2' & \Phi_3' & \Phi_4' \\ \frac{(E_pI_p+2t_4)(\kappa G_pA_p+2t)}{(\kappa G_pA_p-k_1)(\kappa G_pA_p+k_3)}\Phi_1''' + \left(-\frac{(E_pI_p+2t_4)k}{(\kappa G_pA_p+k_3)(\kappa G_pA_p-k_1)}+\frac{(\kappa G_pA_p-k_1)}{(\kappa G_pA_p+k_3)}+\frac{(\kappa G_pA_p+2t)}{(-\kappa G_pA_p+k_2)}\right)\Phi_1' & . & . & . \\ \frac{(E_pI_p+2t_4)}{(\kappa G_pA_p-k_1)}(\kappa G_pA_p+2t)\Phi_1'' + \left(-\frac{(E_pI_p+2t_4)}{(\kappa G_pA_p-k_1)}k+(-k_1+k_2)\right)\Phi_1 & . & . & . \end{bmatrix}^{(i+1)}_{z=z_i}\begin{bmatrix}C_1\\ C_2\\ C_3\\ C_4\end{bmatrix}^{(i+1)}_{z=z_i}.$$

At the pile end:

Fixed end:

$$\begin{aligned} &w_{z=L_p} = 0\\ &\tfrac{dw}{dz}_{z=L_p} = 0\end{aligned} \quad (A7)$$

where $\begin{bmatrix}\Phi_1\\ \Phi_2\\ \Phi_3\\ \Phi_4\end{bmatrix}^T_{z=0}\begin{bmatrix}C_1\\ C_2\\ C_3\\ C_4\end{bmatrix}^{(n)}_{z=L_p} = 0$, and $\begin{bmatrix}\Phi_1'\\ \Phi_2'\\ \Phi_3'\\ \Phi_4'\end{bmatrix}^T_{z=0}\begin{bmatrix}C_1\\ C_2\\ C_3\\ C_4\end{bmatrix}^{(n)}_{z=L_p} = 0\,.$

Free end:

$$\begin{aligned} &\left\{\kappa G_pA_p\left(\tfrac{dw}{dz}-\phi\right)+\{k_2\phi+2t\tfrac{dw}{dz}\}\right\}_{n,z=L_p} = \left\{k_{2end}\phi+2t_{end}\tfrac{dw}{dz}\right\}_{n+1,z=L_p}\\ &\left\{E_pI_p\tfrac{d\phi}{dz}+(-k_1+k_2)w+2t_4\tfrac{d\phi}{dz}\right\}_{n,z=L_p} = \left\{(-k_{1end}+k_{2end})w+2t_{4end}\tfrac{d\phi}{dz}\right\}_{n+1,z=L_p}\end{aligned} \quad (A8)$$

where $\frac{\pi}{2}\int_{r_p}^{\infty}G_s(\phi_r^2+\phi_\theta^2)rdrdr + \frac{\pi}{2}G_sr_p^2 = t_{end}$, $\pi\int_{r_p}^{\infty}\{G_sr_p\frac{d\phi_z}{dr}\phi_r + G_s\frac{r_p}{r}\phi_z\phi_\theta - \lambda_sr_p\phi_z\frac{d\phi_r}{dr} - \lambda_sr_p\phi_z\frac{\phi_r-\phi_\theta}{r}\}rdr + \pi G_sr_p^2 = k_{1end}$, $\pi\int_{rp}^{\infty}\{G_s\{\frac{\phi_z}{r}\phi_\theta + \frac{d\phi_z}{dr}\phi_r\}r_prdr + \pi G_sr_p^2 = k_{2end}$, $\pi\int_{rp}^{\infty}\{[G_s\frac{d\phi_z}{dr}\frac{d\phi_z}{dr} + G_s\frac{\phi_z}{r}\frac{\phi_z}{r}]r_p^2rdr + \pi G_sr_p^2 = k_{3end}$, $\frac{\pi}{2}\int_{rp}^{\infty}(\lambda_s+2G_s)\phi_z^2r_p^2rdr + (\lambda_s+2G_s)$

$$\frac{\pi}{8}r_p^4 = t_{4end}, \quad \text{and} \quad \begin{bmatrix} \left(\eta_3\Phi_1''' + \eta_4\Phi_1' - 2t_{end}\eta_1\Phi_1\right)_{n,z=L_p} \\ \left(\eta_3\Phi_2''' + \eta_4\Phi_2' - 2t_{end}\eta_1\Phi_2\right)_{n,z=L_p} \\ \left(\eta_3\Phi_3''' + \eta_4\Phi_3' - 2t_{end}\eta_1\Phi_3\right)_{n,z=L_p} \\ \left(\eta_3\Phi_4''' + \eta_4\Phi_4' - 2t_{end}\eta_1\Phi_4\right)_{n,z=L_p} \end{bmatrix}^T \begin{bmatrix} C_1 \\ C_2 \\ C_3 \\ C_4 \end{bmatrix}_{z=L_p}^{(n)} = 0,$$

$$\begin{bmatrix} \eta_7\Phi_1''' + \eta_8\Phi_4'' + \eta_9\Phi_1' + \eta_{10}\Phi_1 \\ \eta_7\Phi_2''' + \eta_8\Phi_4'' + \eta_9\Phi_2' + \eta_{10}\Phi_2 \\ \eta_7\Phi_3''' + \eta_8\Phi_3'' + \eta_9\Phi_3' + \eta_{10}\Phi_3 \\ \eta_7\Phi_4''' + \eta_8\Phi_4'' + \eta_9\Phi_4' + \eta_{10}\Phi_4 \end{bmatrix}^T \begin{bmatrix} C_1 \\ C_2 \\ C_3 \\ C_4 \end{bmatrix}_{z=L_p}^{(n)} = 0,$$

$$\eta_1 = -a + \frac{(b-a)\left(\frac{2t_{4end}}{k_{3end}}\frac{2t_{end}}{k_{1end}}a^3 - \left(-\frac{k_{1end}}{k_{3end}} + \frac{2t_{4end}}{k_{3end}}\frac{k}{k_{1end}}\right)a\right)}{\left(\left(\frac{2t_{4end}}{k_{3end}}\frac{2t_{end}}{k_{1end}}(b^3-a^3) - \left(-\frac{k_{1end}}{k_{3end}} + \frac{2t_{4end}}{k_{3end}}\frac{k}{k_{1,end}}\right)(b-a)\right)\right)},$$

$$\eta_2 = -(b-a)\frac{1}{\left(\left(\frac{2t_{4end}}{k_{3end}}\frac{2t_{end}}{k_{1end}}(b^3-a^3) - \left(-\frac{k_{1end}}{k_{3end}} + \frac{2t_{4end}}{k_{3end}}\frac{k}{k_{1end}}\right)(b-a)\right)\right)},$$

$$\eta_3 = \left(-\kappa G_p A_p + k_2 - k_{2end} - 2t_{end}\eta_2\right)\frac{\left(E_pI_p+2t_4\right)\left(\kappa G_pA_p+2t\right)}{\left(\kappa G_pA_p+k_3\right)\left(\kappa G_pA_p-k_1\right)},$$

$$\eta_4 = \left(-\kappa G_p A_p + k_2 - k_{2end} - 2t_{end}\eta_2\right)\left(-\frac{\left(E_pI_p+2t_4\right)k}{\left(\kappa G_pA_p+k_3\right)\left(\kappa G_pA_p-k_1\right)} + \frac{\left(\kappa G_pA_p-k_1\right)}{\left(\kappa G_pA_p+k_3\right)}\right) + \kappa G_pA_p + 2t,$$

$$\eta_5 = a^2 - \left(-a^2+b^2\right)\frac{\left(\frac{2t_{4end}}{k_{3end}}\frac{2t_{end}}{k_{1end}}a^3 - \left(-\frac{k_{1end}}{k_{3end}} + \frac{2t_{4end}}{k_{3end}}\frac{k}{k_{1end}}\right)a\right)}{\left(\left(\frac{2t_{4end}}{k_{3end}}\frac{2t_{end}}{k_{1end}}(b^3-a^3) - \left(-\frac{k_{1end}}{k_{3end}} + \frac{2t_{4end}}{k_{3end}}\frac{k}{k_{1end}}\right)(b-a)\right)\right)},$$

$$\eta_6 = \frac{\left(-a^2+b^2\right)}{\left(\left(\frac{2t_{4end}}{k_{3end}}\frac{2t_{end}}{k_{1end}}(b^3-a^3) - \left(-\frac{k_{1end}}{k_{3end}} + \frac{2t_{4end}}{k_{3end}}\frac{k}{k_{1end}}\right)(b-a)\right)\right)}, \ \eta_7 = \frac{2t_{end}2t_{4end}}{k_{1,end}}\eta_6\frac{\left(E_pI_p+2t_4\right)\left(\kappa G_pA_p+2t\right)}{\left(\kappa G_pA_p+k_3\right)\left(\kappa G_pA_p-k_1\right)},$$

$$\eta_8 = \frac{\left(E_pI_p+2t_4\right)}{\left(\kappa G_pA_p-k_1\right)}\left(\kappa G_pA_p+2t\right), \ \eta_9 = \frac{2t_{end}2t_{4end}}{k_{1,end}}\eta_6\left(-\frac{\left(E_pI_p+2t_4\right)k}{\left(\kappa G_pA_p+k_3\right)\left(\kappa G_pA_p-k_1\right)} + \frac{\left(\kappa G_pA_p-k_1\right)}{\left(\kappa G_pA_p+k_3\right)}\right),$$

$$\eta_{10} = -\frac{\left(E_pI_p+2t_4\right)}{\left(\kappa G_pA_p-k_1\right)}k + \left(-k_1+k_2\right) - \left(-k_{1end}+k_{2end}\right) + \frac{2t_{end}2t_{4end}}{k_{1,end}}\eta_5 - \frac{2kt_{4end}}{k_{1,end}},$$

$$a = \sqrt{\widetilde{t} + \sqrt{\widetilde{t}^2 - \widetilde{k}}}, b = \sqrt{\widetilde{t} - \sqrt{\widetilde{t}^2 - \widetilde{k}}}, \widetilde{t} = \frac{k_{3,end}2t_{end} + 2t_{4,end}k - k_{1,end}^2}{8t_{4,end}t_{end}}, \widetilde{k} = \frac{k_{3,end}k}{2t_{4,end}2t_{end}}.$$

For the soil area at $z > L_p$, the governing differential equations are given by:

$$\begin{aligned} 2t_{end}\frac{d^2w}{dz^2} + k_{1end}\frac{d\phi}{dz} - kw &= 0 \\ -k_{3end}\phi - k_{1end}\frac{dw}{dz} + 2t_{4end}\frac{d^2\phi}{dz^2} &= 0 \end{aligned} \tag{A9}$$

where $w_{z=L_p^-} = w_{z=L_p^+}$, and $\phi_{z=L_p^-} = \phi_{z=L_p^+}$, therefore, the solution of Equation (11) is given as:

$$w = C_1e^{-az} + C_2e^{-bz} \tag{A10}$$

$$\text{where} \quad C_1 = \left(w_{z=L_p} - \frac{\phi_{z=L_p} - \left(\frac{2t_{4,end}}{k_{3,end}}\frac{2t_{end}}{k_{1,end}}a^3 - \left(-\frac{k_{1,end}}{k_{3,end}} + \frac{2t_{4,end}}{k_{3,end}}\frac{k}{k_{1,end}}\right)a\right)w_{z=Lp}}{\left(\left(\frac{2t_{4,end}}{k_{3,end}}\frac{2t_{end}}{k_{1,end}}(b^3-a^3) - \left(-\frac{k_{1,end}}{k_{3,end}} + \frac{2t_{4,end}}{k_{3,end}}\frac{k}{k_{1,end}}\right)(b-a)\right)\right)}\right)e^{aL_p},$$

$$C_2 = \frac{\phi_{z=L_p} - \left(\frac{2t_{4,end}}{k_{3,end}}\frac{2t_{end}}{k_{1,end}}a^3 - \left(-\frac{k_{1,end}}{k_{3,end}} + \frac{2t_{4,end}}{k_{3,end}}\frac{k}{k_{1,end}}\right)a\right)w_{z=Lp}}{\left(\left(\frac{2t_{4,end}}{k_{3,end}}\frac{2t_{end}}{k_{1,end}}(b^3-a^3) - \left(-\frac{k_{1,end}}{k_{3,end}} + \frac{2t_{4,end}}{k_{3,end}}\frac{k}{k_{1,end}}\right)(b-a)\right)\right)}e^{bL_p}.$$

Appendix C

As mentioned previously, the governing differential equations for the soil surrounding the deep foundation can be obtained. The governing differential equations for the functions ϕ_r are:

$$\frac{d^2\phi_r}{dr^2} + \frac{1}{r}\frac{d\phi_r}{dr} - \left(\left(\frac{\gamma_1}{r}\right)^2 + \left(\frac{\gamma_2}{r_p}\right)^2\right)\phi_r = \frac{\gamma_3^2}{r}\frac{d\phi_\theta}{dr} - \left(\frac{\gamma_1}{r}\right)^2\phi_\theta + \gamma_0^2\frac{d\phi_z}{dr} \tag{A11}$$

$$\text{where} \quad \gamma_0 = \sqrt{\frac{\int_0^\infty \left(G_s \phi r_p \frac{dw}{dz} r - \lambda_s \frac{d\phi}{dz} r_p w r \right) dz}{\int_0^\infty (\lambda_s + 2G_s) w w dz}}, \gamma_1 = \sqrt{\frac{\int_0^\infty (\lambda_s + 3G_s) w w dz}{\int_0^\infty (\lambda_s + 2G_s) w w dz}},$$

$$\gamma_2 = r_p \sqrt{\frac{\int_0^\infty G_s \frac{dw}{dz} \frac{dw}{dz} dz}{\int_0^\infty (\lambda_s + 2G_s) w w dz}}, \gamma_3 = \sqrt{\frac{\int_0^\infty (G_s + \lambda_s) w w dz}{\int_0^\infty (\lambda_s + 2G_s) w w dz}}.$$

The governing differential equations for the functions ϕ_θ are:

$$\frac{d^2\phi_\theta}{dr^2} + \frac{1}{r}\frac{d\phi_\theta}{dr} - \left(\frac{\gamma_4}{r}\right)^2 \phi_\theta - \left(\frac{\gamma_5}{r_p}\right)^2 \phi_\theta = -\frac{\gamma_6^2}{r}\frac{d\phi_r}{dr} - \left(\frac{\gamma_4}{r}\right)^2 \phi_r + \frac{\gamma_7^2}{r}\phi_z \tag{A12}$$

$$\text{where } \gamma_4 = \sqrt{\frac{\int_0^\infty (\lambda_s + 3G_s) w w dz}{\int_0^\infty G_s w w dz}}, \gamma_5 = r_p \sqrt{\frac{\int_0^\infty G_s \frac{dw}{dz} \frac{dw}{dz} dz}{\int_0^\infty G_s w w dz}}, \gamma_6 = \sqrt{\frac{\int_0^\infty (G_s + \lambda_s) w w dz}{\int_0^\infty G_s w w dz}},$$

$$\gamma_7 = \sqrt{\frac{\int_0^\infty \left(G_s \phi r_p \frac{dw}{dz} - \lambda_s \frac{d\phi}{dz} r_p w \right) dz}{\int_0^\infty G_s w w dz}}.$$

The governing differential equations for the functions ϕ_z are:

$$\frac{d^2\phi_z}{dr^2} + \frac{1}{r}\frac{d\phi_z}{dr} - (\gamma_9^2 + \frac{1}{r^2})\phi_z = -\gamma_8^2 \frac{d\phi_r}{dr} - \frac{1}{r}\gamma_8^2 \phi_r + \frac{1}{r}\gamma_8^2 \phi_\theta \tag{A13}$$

$$\text{where } \gamma_8 = \sqrt{\frac{\int_0^\infty \left(G_s \phi \frac{dw}{dz} - \lambda_s \frac{d\phi}{dr} w \right) dz}{\int_0^\infty G_s \phi r_p \phi dz}}, \gamma_9 = \sqrt{\frac{\int_0^\infty (\lambda_s + 2G_s) \frac{d\phi}{dr}\frac{d\phi}{dr} dz}{\int_0^\infty G_s \phi \phi dz}}.$$

The relationship among ϕ_r, ϕ_θ, and ϕ_z can be described as follows:

$$\begin{aligned}
\phi_r &= \left[K_{\phi r} - CK_{\phi z}^{-1} M - (B + CK_{\phi z}^{-1} N)(K_{\phi\theta} - FK_{\phi z}^{-1} N)^{-1} (E + FK_{\phi z}^{-1} M) \right]^{-1} \left[A + CK_{\phi z}^{-1} G + (B + CK_{\phi z}^{-1} N)(K_{\phi\theta} - FK_{\phi z}^{-1} N)^{-1} (D + FK_{\phi z}^{-1} G) \right] \\
\phi_\theta &= (K_{\phi\theta} - FK_{\phi z}^{-1} N)^{-1} \left[D + FK_{\phi z}^{-1} G + (E + FK_{\phi z}^{-1} M)\phi_r \right] \\
\phi_z &= K_{\phi z}^{-1} G + K_{\phi z}^{-1} M \phi_r + K_{\phi z}^{-1} N \phi_\theta
\end{aligned} \tag{A14}$$

where the matrixes of $\boldsymbol{K_{\phi r}}$, $\boldsymbol{K_{\phi\theta}}$, $\boldsymbol{K_{\phi z}}$, $\boldsymbol{A_m}$, $\boldsymbol{B_m}$, $\boldsymbol{C_m}$, $\boldsymbol{P}$, $\boldsymbol{E}$, $\boldsymbol{Q}$, $\boldsymbol{G}$, $\boldsymbol{M}$, and $\boldsymbol{N}$ are given as following:

$$K_{\phi_r}=\begin{bmatrix}
\begin{matrix}1&0&\cdots&\\0&1&0&\\\vdots&\vdots&\vdots&\\0&\cdots&&1\end{matrix} & 0\le r\le r_{\mathrm{P}} & \cdots & & & & & 0\\
0\ \cdots\ \frac{1}{\Delta r^2}-\frac{1}{r}\frac{1}{2\Delta r} & -\left(\frac{2}{\Delta r^2}+\left(\frac{\gamma_1}{r}\right)^2+\left(\frac{\gamma_2}{rp}\right)^2\right) & \frac{1}{\Delta r^2}+\frac{1}{r}\frac{1}{2\Delta r} & & & & & \\
 & \frac{1}{\Delta r^2}-\frac{1}{r}\frac{1}{2\Delta r} & -\left(\frac{2}{\Delta r^2}+\left(\frac{\gamma_1}{r}\right)^2+\left(\frac{\gamma_2}{rp}\right)^2\right) & \frac{1}{\Delta r^2}+\frac{1}{r}\frac{1}{2\Delta r} & & & & \\
 & & & & & & & \\
 & & & & & \frac{1}{\Delta r^2}-\frac{1}{r}\frac{1}{2\Delta r} & -\left(\frac{2}{\Delta r^2}+\left(\frac{\gamma_1}{r}\right)^2+\left(\frac{\gamma_2}{rp}\right)^2\right) & \frac{1}{\Delta r^2}+\frac{1}{r}\frac{1}{2\Delta r}\\
 & & & & \cdots & 0 & 0 & 1
\end{bmatrix}_{4n\times 4n}$$

$$A=D=\left[\underbrace{1\ \ \cdots\ \ 1}_{0\le r\le r_{\mathrm{P}}}\ \ 0\ \ \cdots\ \ 0\ \ 0\right]^T$$

$$B=\begin{bmatrix}
\begin{matrix}0&0&\cdots&\\0&0&0&\\\vdots&\vdots&\vdots&\\0&\cdots&&0\end{matrix} & 0\le r\le r_{\mathrm{P}} & \cdots & & & & & 0\\
0\ \cdots\ -\frac{\gamma_3^2}{r}\frac{1}{2\Delta r} & -\left(\frac{\gamma_1}{r}\right)^2 & \frac{\gamma_3^2}{r}\frac{1}{2\Delta r} & & & & & \\
 & -\frac{\gamma_3^2}{r}\frac{1}{2\Delta r} & -\left(\frac{\gamma_1}{r}\right)^2 & \frac{\gamma_3^2}{r}\frac{1}{2\Delta r} & & & & \\
 & & & & & & & \\
 & & & & & -\frac{\gamma_3^2}{r}\frac{1}{2\Delta r} & -\left(\frac{\gamma_1}{r}\right)^2 & \frac{\gamma_3^2}{r}\frac{1}{2\Delta r}\\
 & & & & \cdots & 0 & 0 & 0
\end{bmatrix}_{4n\times 4n}$$

$$C=\begin{bmatrix}
\begin{matrix}0&0&\cdots&\\0&0&0&\\\vdots&\vdots&\vdots&\\0&\cdots&&0\end{matrix} & 0\le r\le r_{\mathrm{P}} & \cdots & & & & & 0\\
0\ \cdots\ -\frac{\gamma_0^2}{2\Delta r} & 0 & +\frac{\gamma_0^2}{2\Delta r} & & & & & \\
 & -\frac{\gamma_0^2}{2\Delta r} & 0 & +\frac{\gamma_0^2}{2\Delta r} & & & & \\
 & & & & & & & \\
 & & & & & -\frac{\gamma_0^2}{2\Delta r} & 0 & \frac{\gamma_0^2}{2\Delta r}\\
 & & & & \cdots & 0 & 0 & 0
\end{bmatrix}_{4n\times 4n}$$

$$K_{\phi_\theta}=\begin{bmatrix}
\begin{matrix}1&0&\cdots&\\0&1&0&\\\vdots&\vdots&\vdots&\\0&\cdots&&1\end{matrix} & 0\le r\le r_{\mathrm{P}} & \cdots & & & & & 0\\
0\ \cdots\ \frac{1}{\Delta r^2}-\frac{1}{r}\frac{1}{2\Delta r} & -\left(\frac{2}{\Delta r^2}+\left(\frac{\gamma_4}{r}\right)^2+\left(\frac{\gamma_5}{r_p}\right)^2\right) & \frac{1}{\Delta r^2}+\frac{1}{r}\frac{1}{2\Delta r} & & & & & \\
 & \frac{1}{\Delta r^2}-\frac{1}{r}\frac{1}{2\Delta r} & -\left(\frac{2}{\Delta r^2}+\left(\frac{\gamma_4}{r}\right)^2+\left(\frac{\gamma_5}{r_p}\right)^2\right) & \frac{1}{\Delta r^2}+\frac{1}{r}\frac{1}{2\Delta r} & & & & \\
 & & & & & & & \\
 & & & & & \frac{1}{\Delta r^2}-\frac{1}{r}\frac{1}{2\Delta r} & -\left(\frac{2}{\Delta r^2}+\left(\frac{\gamma_4}{r}\right)^2+\left(\frac{\gamma_5}{r_p}\right)^2\right) & \frac{1}{\Delta r^2}+\frac{1}{r}\frac{1}{2\Delta r}\\
 & & & & \cdots & 0 & 0 & 1
\end{bmatrix}_{4n\times 4n}$$

$$E=\begin{bmatrix}
\boxed{\begin{matrix}0&0&\cdots&0\\0&0&0&\vdots\\\vdots&\vdots&\vdots&\vdots\\0&\cdots&0&0\end{matrix}} & \begin{matrix}\cdots&\cdots&\cdots&\cdots&0\\\cdots&\cdots&\cdots&\cdots&0\\\cdots&\cdots&\cdots&\cdots&\vdots\\\cdots&\cdots&\cdots&\cdots&\vdots\end{matrix} \\
\begin{matrix}0\\0\\\vdots\\0\end{matrix} & \begin{matrix}\cdots&\cdots&\cdots&\cdots&0\\\cdots&\cdots&\cdots&\cdots&0\\\cdots&\cdots&\cdots&\cdots&\vdots\\\cdots&\cdots&\cdots&\cdots&\vdots\end{matrix}
\end{bmatrix}$$

$0\le r\le r_{\mathrm{p}}$

$$\begin{bmatrix}
0 & \cdots & \frac{\gamma_6^2}{r}\frac{1}{2\Delta r} & -\left(\frac{\gamma_4}{r}\right)^2 & -\frac{\gamma_6^2}{r}\frac{1}{2\Delta r} & & & \\
 & & \frac{\gamma_6^2}{r}\frac{1}{2\Delta r} & -\left(\frac{\gamma_4}{r}\right)^2 & -\frac{\gamma_6^2}{r}\frac{1}{2\Delta r} & & & \\
 & & & & & \frac{\gamma_6^2}{r}\frac{1}{2\Delta r} & -\left(\frac{\gamma_4}{r}\right)^2 & -\frac{\gamma_6^2}{r}\frac{1}{2\Delta r} \\
 & & & & & 0 & 0 & 0
\end{bmatrix}_{4n\times 4n}$$

$$F=\begin{bmatrix}
\boxed{\begin{matrix}0&0&\cdots&0\\0&0&0&\vdots\\\vdots&\vdots&\vdots&\vdots\\0&\cdots&0&0\end{matrix}} & \begin{matrix}\cdots&\cdots&\cdots&0\\\cdots&\cdots&\cdots&0\\\cdots&\cdots&\cdots&\vdots\\\cdots&\cdots&\cdots&\vdots\end{matrix} \\
\begin{matrix}0\\0\\\vdots\\0\end{matrix} & \begin{matrix}\cdots&\cdots&\cdots&0\\\cdots&\cdots&\cdots&0\\\cdots&\cdots&\cdots&\vdots\\\cdots&\cdots&\cdots&\vdots\end{matrix}
\end{bmatrix}$$

$0\le r\le r_{\mathrm{p}}$

$$\begin{bmatrix}
0 & \cdots & \frac{\gamma_7^2}{r} & 0 & & & & \\
 & & 0 & \frac{\gamma_7^2}{r} & 0 & & & \\
 & & & & & 0 & \frac{\gamma_7^2}{r} & 0 \\
 & & & & & 0 & 0 & 0
\end{bmatrix}_{4n\times 4n}$$

$$K_{\phi_z}=\begin{bmatrix}
\boxed{\begin{matrix}1&0&0&\cdots\\0&1&0&\vdots\\\vdots&\vdots&\vdots&\vdots\\\cdots&0&1\end{matrix}} & \begin{matrix}\cdots&\cdots&\cdots&\cdots\\\cdots&\cdots&\cdots&\cdots\\\cdots&\cdots&\cdots&\cdots\\\cdots&\cdots&\cdots&\cdots\end{matrix} \\
\begin{matrix}0\\0\\\vdots\\0\end{matrix} & \begin{matrix}\cdots&\cdots&\cdots&\cdots\\\cdots&\cdots&\cdots&\cdots\\\cdots&\cdots&\cdots&\cdots\\\cdots&\cdots&\cdots&\cdots\end{matrix}
\end{bmatrix}$$

$0\le r\le r_{\mathrm{p}}$

$$\begin{bmatrix}
\cdots & 0 & \frac{1}{\Delta r^2}-\frac{1}{r}\frac{1}{2\Delta r} & -\left(\frac{1}{\Delta r^2}+\gamma_9^2+\frac{1}{r^2}\right) & \frac{1}{\Delta r^2}+\frac{1}{r}\frac{1}{2\Delta r} & & & \\
 & & \frac{1}{\Delta r^2}-\frac{1}{r}\frac{1}{2\Delta r} & -\left(\frac{1}{\Delta r^2}+\gamma_9^2+\frac{1}{r^2}\right) & \frac{1}{\Delta r^2}+\frac{1}{r}\frac{1}{2\Delta r} & 0 & & \\
 & & 0 & \frac{1}{\Delta r^2}-\frac{1}{r}\frac{1}{2\Delta r} & -\left(\frac{1}{\Delta r^2}+\gamma_9^2+\frac{1}{r^2}\right) & \frac{1}{\Delta r^2}+\frac{1}{r}\frac{1}{2\Delta r} & & \\
\cdots & 0 & 0 & 0 & 0 & 1
\end{bmatrix}_{4n\times 4n}$$

$$G=\begin{bmatrix}\underbrace{0 & \frac{\Delta r}{r_p} & \frac{2\Delta r}{r_p} & \cdots & \frac{r_p}{r_p}}_{0\le r\le r_{\mathrm{p}}} & 0\cdots & 0\end{bmatrix}^T$$

$$M=\begin{bmatrix}
0&0&0&\cdots&\cdots&\cdots&\cdots&\cdots&\cdots\\
0&0&0&0&\cdots&\cdots&\cdots&\cdots&\cdots\\
0&0&0&0&0&\cdots&\cdots&\cdots&\cdots\\
0&0&0&\frac{\gamma_8^2}{2\Delta r}&-\frac{\gamma_8^2}{r}&-\frac{\gamma_8^2}{2\Delta r}&\cdots&\cdots&\cdots\\
\cdots&\cdots&\cdots&\cdots&\cdots&\cdots&\cdots&\cdots&\cdots\\
\cdots&\cdots&\cdots&\cdots&\cdots&\cdots&\cdots&\cdots&\cdots\\
\cdots&\cdots&\cdots&\cdots&0&\frac{\gamma_8^2}{2\Delta r}&-\frac{\gamma_8^2}{r}&-\frac{\gamma_8^2}{2\Delta r}&0\\
\cdots&\cdots&\cdots&\cdots&\cdots&0&\frac{\gamma_8^2}{2\Delta r}&-\frac{\gamma_8^2}{r}&-\frac{\gamma_8^2}{2\Delta r}\\
0&\cdots&\cdots&0&0&0&0&0&1
\end{bmatrix}_{4n\times 4n}$$

$$N=\begin{bmatrix}
0&0&0&\cdots&\cdots&\cdots&\cdots&\cdots&\cdots\\
0&0&0&0&\cdots&\cdots&\cdots&\cdots&\cdots\\
0&0&0&0&0&\cdots&\cdots&\cdots&\cdots\\
0&0&0&\frac{\gamma_8^2}{r}&0&\cdots&\cdots&\cdots&\cdots\\
\cdots&\cdots&\cdots&\cdots&\frac{\gamma_8^2}{r}&\cdots&\cdots&\cdots&\cdots\\
\cdots&\cdots&\cdots&\cdots&\cdots&\cdots&\cdots&\cdots&\cdots\\
\cdots&\cdots&\cdots&\cdots&&0&\frac{\gamma_8^2}{r}&0&0\\
\cdots&\cdots&\cdots&\cdots&\cdots&&0&\frac{\gamma_8^2}{r}&0\\
0&\cdots&\cdots&0&0&0&0&0&0
\end{bmatrix}_{4n\times 4n}$$

The above calculation is conducted in MATLAB (Figure A1).

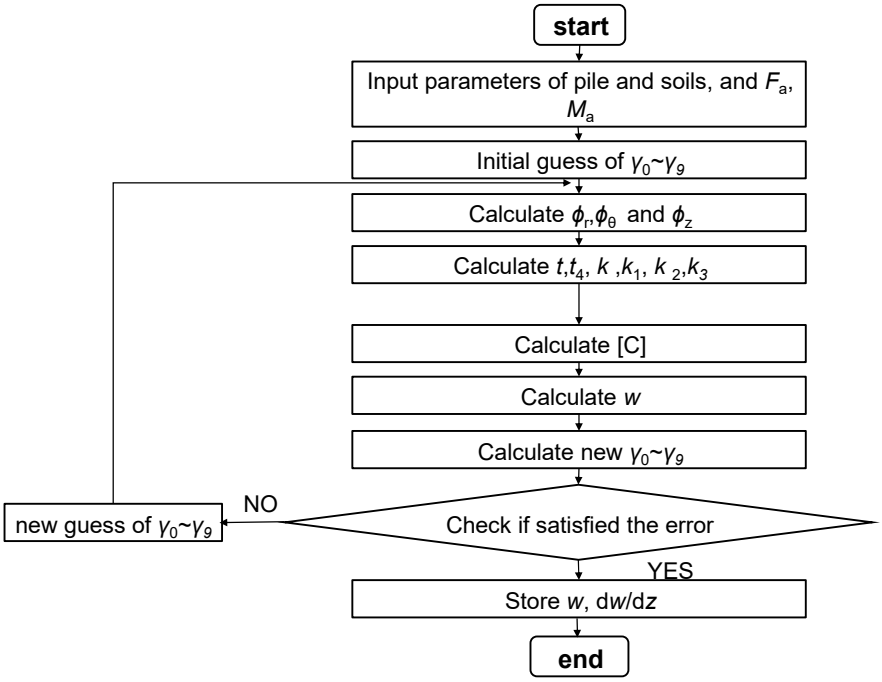

Figure A1. Flow chart of the iterative algorithm in MATLAB [55].

References

1. Qin, W.; Cai, S.; Dai, G.; Wang, D.; Chang, K. Soil Resistance during Driving of Offshore Large-Diameter Open-Ended Thin-Wall Pipe Piles Driven into Clay by Impact Hammers. *Comput. Geotech.* **2023**, *153*, 105085. [CrossRef]
2. Qin, W.; Cai, S.; Dai, G.; Wei, H. Analytical solutions of soil plug behaviors in open-ended pile driven by impact load. *Acta Geotech.* **2023**, *18*, 4183–4194. [CrossRef]
3. Qin, W.; Gao, J.; Chang, K.; Dai, G.; Wei, H. Set-up effect of large-diameter open-ended thin-walled pipe piles driven in clay. *Comput. Geotech.* **2023**, *159*, 105459. [CrossRef]
4. Wu, J.-S.; Hsu, S.-H. A unified approach for the free vibration analysis of an elastically supported immersed uniform beam carrying an eccentric tip mass with rotary inertia. *J. Sound Vib.* **2006**, *291*, 1122–1147. [CrossRef]
5. Galvín, P.; Romero, A.; Solís, M.; Domínguez, J. Dynamic characterisation of wind turbine towers account for a monopile foundation and different soil conditions. *Struct. Infrastruct. Eng.* **2016**, *13*, 942–954. [CrossRef]
6. Wang, P.; Zhao, M.; Du, X.; Liu, J.; Xu, C. Wind, wave and earthquake responses of offshore wind turbine on monopile foundation in clay. *Soil Dyn. Earthq. Eng.* **2018**, *113*, 47–57. [CrossRef]
7. Arany, L.; Bhattacharya, S.; John, M.; Hogan, S.J. Design of monopiles for offshore wind turbines in 10 steps. *Soil Dyn. Earthq. Eng.* **2017**, *92*, 126–152. [CrossRef]
8. Subhamoy, B. *Design of Foundations for Offshore Wind Turbines*; John Wiley & Sons Ltd.: West Sussex, UK, 2017. Available online: https://lccn.loc.gov/2018046931 (accessed on 16 February 2024).
9. Hu, Q.; Han, F.; Prezzi, M.; Salgado, R.; Zhao, M. Lateral load response of large-diameter monopiles in sand. *Géotechnique* **2021**, *72*, 1035–1050. [CrossRef]
10. Hu, Q.; Han, F.; Prezzi, M.; Salgado, R.; Zhao, M. Finite-element analysis of the lateral load response of monopiles in layered sand. *J. Geotech. Geoenviron. Eng.* **2022**, *148*, 04022001. [CrossRef]
11. Bergfelt, A. The axial and lateral loading bearing capacity, and failure by buckling of piles in soft clay. In Proceedings of the 4th International Conference on Soil Mechanics and Foundation Engineering, London, UK, 12–14 August 1957; Volume 2, pp. 8–19.
12. Thomas, G. *Determination of Spring Constant, Term Project*; Rensselaer Polytechnic Institute: Troy, NY, USA, 1978.
13. Randolph, M. The response of flexible piles to lateral loading. *Geotechnique* **1981**, *2*, 247–259. [CrossRef]
14. Poulos, H.; Davis, E. *Pile Foundation Analysis and Design*; Rainbow-Bridge Book Co.: Landon, UK, 1980.
15. Barber, E.S. Discussion to paper by S. M. Gleser. *ASTM Spec. Tech. Publ.* **1953**, *154*, 96–99.
16. Budhu, M.; Davies, G. Analysis of Laterally Loaded Piles in Soft Clays. *J. Geotech. Eng.* **1988**, *114*, 21. [CrossRef]
17. Pender, M.J. ASeismic Pile Foundation Design Analysis. *Bull. N. Z. Natl. Soc. Earthq. Eng.* **1993**, *26*, 49–161. [CrossRef]
18. Gazetas, G. Seismic response of end-bearing single piles. *Int. J. Soil Dyn. Earthq. Eng.* **1984**, *3*, 82–93. [CrossRef]
19. Higgins, W.; Vasquez, C.; Basu, D.; Griffiths, D.V. Elastic solutions for laterally loaded piles. *J. Geotech. Geoenviron. Eng.* **2013**, *139*, 1096–1103. [CrossRef]
20. Shadlou, M.; Bhattacharya, S. Dynamic stiffness of monopiles supporting offshore wind turbine generators. *Soil Dyn. Earthq. Eng.* **2016**, *8*, 15–32. [CrossRef]

21. Aissa, M.; Bouzid, D.A.; Bhattacharya, S. Monopile head stiffness for serviceability limit state calculations in assessing the natural frequency of offshore wind turbines. *Int. J. Geotech. Eng.* **2017**, *6*, 267–283. [CrossRef]
22. Anoyatis, G.; Lemnitzer, A. Dynamic pile impedances for laterally-loaded piles using improved Tajimi and Winkler formulations. *Soil Dyn. Earthq. Eng.* **2017**, *92*, 279–297. [CrossRef]
23. Rao, S.S. *Vibration of Continuous Systems*; John Wiley & Sons, Inc.: Hoboken, NJ, USA, 2007.
24. Ko, Y.; Li, Y. Response of a scale-model pile group for a jacket foundation of an offshore wind turbine in liquefiable ground during shaking table tests. *Earthq. Eng. Struct. Dyn.* **2020**, *49*, 1682–1701. [CrossRef]
25. European Committee for Standardization. *Eurocode 8: Design of Structures for Earthquake Resistance—Part 5: Foundations, Retaining Structures and Geotechnical Aspects*; European Committee for Standardization: Brussels, Belgium, 2003.
26. Syngros, C. Seismic Response of Piles and pile-Supported Bridge Piers Evaluated through Case Histories. Ph.D. Thesis, City University of New York, New York, NY, USA, 2004.
27. Carter, J.; Kulhawy, F. Analysis of laterally loaded shafts in rock. *J. Geotech. Eng.* **1992**, *118*, 839–855. [CrossRef]
28. Bouzid, D.A.; Bhattacharya, S.; Otsmane, L. Assessment of natural frequency of installed offshore wind turbines using nonlinear finite element model considering soil-monopile interaction. *J. Rock Mech. Geotech. Eng.* **2018**, *10*, 333–346. [CrossRef]
29. Abed, Y.; Bouzid, D.A.; Bhattacharya, S. Static impedance functions for monopiles supporting offshore wind turbines in nonhomogeneous soils emphasis on soil/monopile interface characteristics. *Earthq. Struct.* **2016**, *10*, 1143–1179. [CrossRef]
30. Salgado, R.; Tehrani, F.S.; Prezzi, M. Analysis of laterally loaded pile groups in multilayered elastic soil. *Comput. Geotech.* **2014**, *62*, 136–153. [CrossRef]
31. Han, F. Axial and Lateral Resistance of Non-Displacement Piles. Ph.D. Thesis, Purdue University, West Lafayette, IN, USA, 2017.
32. Han, F.; Prezzi, M.; Salgado, R. Energy-based solutions for non-displacement piles subjected to lateral loads. *Int. J. Geomech.* **2017**, *17*, 04017104. [CrossRef]
33. Byrne, B.W.; Burd, H.J.; Houlsby, G.T. New Design Methods for Large Diameter Piles under Lateral Loading for Offshore Wind Applications. In Proceedings of the Third International Symposium on Frontiers in Offshore Geotechnics ISFOG, Oslo, Norway, 10–12 June 2015.
34. Byrne, B.W.; Mcadam, R.A.; Burd, H.J. Field testing of large diameter piles under lateral loading for offshore wind applications. In Proceedings of the XVI European Conference on Soil Mechanics and Geotechnical Engineering (ECSMGE), Edinburg, UK, 13–17 September 2016; pp. 1255–1260.
35. Gupta, B.K.; Basu, D. Applicability of Timoshenko, Euler–Bernoulli and rigid beam theories in the analysis of laterally loaded monopiles and piles. *Géotechnique* **2018**, *9*, 772–785. [CrossRef]
36. Gupta, B.K.; Basu, D. Offshore wind turbine monopile foundations: Design perspectives. *Ocean Eng.* **2020**, *213*, 107514. [CrossRef]
37. Gupta, B.K. Dynamic pile-head stiffness of laterally loaded end-bearing pile in linear viscoelastic soil—A comparative study. *Comput. Geotech.* **2022**, *145*, 104654. [CrossRef]
38. Cao, G.; Hian, S.; Ding, X. Horizontal static for OWT monopiles based on Timoshenko beam theory. *Int. J. Geomech.* **2023**, *23*, 04023202. [CrossRef]
39. Li, X.; Dai, G.; Zhang, F.; Gong, W. Energy-Based analysis of laterally loaded caissons with large diameters under small-strain conditions. *Int. J. Geomech.* **2022**, *22*, 05022005. [CrossRef]
40. Li, X.; Dai, G. Closure to "Energy-Based Analysis of Laterally Loaded Caissons with Large Diameters under Small-Strain Conditions". *Int. J. Geomech.* **2023**, *23*, 07023008. [CrossRef]
41. Li, X.; Dai, G.; Zhu, M.; Zhu, W.; Zhang, F. Investigation of the soil deformation around late-rally loaded deep foundations with large diameters. *Acta Geotech.* **2023**, *19*, 2293–2314. [CrossRef]
42. Li, X.; Dai, G.; Zhu, M.; Wang, L.; Liu, H. A Simplified Method for Estimating the Initial Stiffness of Monopile—Soil Interaction Under Lateral Loads in Offshore Wind Turbine Systems. *China Ocean Eng.* **2023**, *37*, 165–174. [CrossRef]
43. Li, X.; Zhu, M.; Dai, G.; Wang, L.; Liu, J. Interface Mechanical Behavior of Flexible Piles Under Lateral Loads in OWT Systems. *China Ocean Eng.* **2023**, *3*, 484–494. [CrossRef]
44. Bhattacharya, S.; Carrington, T.; Aldridge, T. Observed increases in offshore piledriving resistance. *Proc. Inst. Civ. Eng.—Geotech. Eng.* **2009**, *162*, 71–80. [CrossRef]
45. Skempton, A.W.; Henkel, D.J. Tests on London Clay fromDeepBorings at Paddington, Victoria, and the South Bank. In Proceedings of the 4th International Conference on Soil Mechanics and Foundation Engineering, London, UK, 12–14 August 1957; Volume 1, pp. 100–106.
46. Ward, W.H.; Marsland, A.; Samuels, S.G. Properties of the London Clay at the Ashford Common Shaft: In-Situ and Undrained Strength Tests. *Geotechnique* **1965**, *15*, 321–344. [CrossRef]
47. Burland, J.B.; Lord, J.A. The Load-Deformation Behavior of the Middle Chalk at Mundford, Norfolk: A Comparison between Full Scale Performance and In-Situ Laboratory Measurements, Building Research Station CP. 1969. Available online: https://eurekamag.com/research/018/258/018258882.php (accessed on 16 February 2024).
48. Butler, F.G. Heavily Over-Consolidated Clays. In *BGS Conference on Settlement of Structures*; Wiley: London, UK, 1974; pp. 531–578. Available online: http://www.geosolve.co.uk/refs/Butler_F_G_1975.pdf (accessed on 16 February 2024).
49. Hobbs, N.B. Factors Affecting the Prediction of Settlement on Rock with Particular Reference to Chalk and Trias. In *BGS Conference on Settlement of Structures*; Wiley: London, UK, 1974; p. 579-560.
50. Selvadurai, P. The Analytical Method in Geomechanics. *Appl. Mech. Rev.* **2007**, *60*, 87–106. [CrossRef]

51. Malekjafarian, A.; Jalilvand, S.; Doherty, P.; Igoe, D. Foundation damping for monopile supported offshore wind turbines: A review. *Mar. Struct.* **2021**, *77*, 102937. Available online: https://www.sciencedirect.com/science/article/pii/S0951833921000058 (accessed on 16 February 2024). [CrossRef]
52. Jalbi, S.; Shadlou, M.; Bhattacharya, S. Impedance functions for rigid skirted caissons supporting offshore wind turbines. *Ocean Eng.* **2018**, *150*, 21–35. [CrossRef]
53. ABAQUS. *Abaqus Analysis User's Manual: ABAQUS 6.15*; SIMULIA: Johnston, RI, USA, 2018.
54. Laszlo, A.; Bhattacharya, S.; Macdonald, J.H.G.; Hogan, S.J. Closed-form solution of Eigen frequency of monopile supported offshore wind turbines in deeper waters incorporating stiffness of substructure and SSI. *Soil Dyn. Earthq. Eng.* **2016**, *83*, 18–32. [CrossRef]
55. The MathWorks Inc. *Optimization Toolbox Version: (R2018b)*; The MathWorks Inc.: Natick, MA, USA, 2018; Available online: https://www.mathworks.com (accessed on 16 February 2024).